MODELLING AND SIMULATION OF THIN FILM FLOW IN POROUS MEDIA

Thesis submitted to the University of Nottingham for the degree of Master of Philosophy

Yakubu Salihu Yakubu

20411018

School of Mathematical Sciences,

Faculty of Science,

University of Nottingham, UK

May 22, 2025

Abstract

This thesis explores the behaviour of thin film flow in both porous and non-porous media, considering both single and two-fluid systems. It establishes a comprehensive mathematical framework to describe the flow dynamics under different physical conditions, aiming to clarify the transition between these two regimes. In the case of porous media, the flow is described by the Brinkman equation, which incorporates the effects of permeability and viscous shear.

On the other hand, the Navier-Stokes equation is used to model flow in non-porous media. The model for porous media seamlessly transitions to the non-porous scenario as the permeability parameter, α approaches zero, ensuring a consistent approach across both domains. Likewise, the two-fluid system simplifies to a single-fluid model when the parameter n, which indicates the viscosity ratio of the fluid, is set to zero.

The thin-film equations are solved numerically with the Chebfun framework, known for its efficient and accurate spectral methods suitable for complex equations. The numerical results examine key parameters such as stability and flow rates and emphasize the relationship between permeability, fluid interactions, and boundary conditions.

Dedication

This study is dedicated to my late father and mother, Alhaji Salihu Yakubu Idris and Hajiya Habiba Salihu Yakubu, may Almighty Allah, the most Gracious, the most Merciful forgive all their shortcomings.

Acknowledgement

I want to thank and express my deepest gratitude to the following, without whom this work would not have been possible.

- I am deeply grateful to the Petroleum Technology Development Fund (PTDF) Nigeria for their generous financial support, which allowed me to conduct my research and complete this thesis, and to the Federal University of Kashere, Gombe state, for granting the study fellowship to embark on this study.

- I sincerely thank my supervisors, Dr. Matteo Icardi and Dr. Anna Kalogirou, for their guidance, patience, and encouragement throughout this process. Their expertise and constructive feedback were instrumental in shaping this work. I also thank Dr. Mirco Magnini for his initial valuable insights and support.

- I am grateful to my family, whose love and encouragement sustained me during challenging times. To my mother, wives, and children, thank you for believing in me and for your endless patience and understanding. I am also grateful to my friends, who provided moral support and cheered me on throughout this journey. To everyone who contributed to this journey in large or small ways, thank you from the bottom of my heart.

Contents

List of Tables

List of Figures

Nomenclature

English/Greek Symbols

α	Parameter in terms of permeability
ϵ	smallest number
γ	Surface tension coefficient
κ	Curvature of the interface
$\mathbb{I}$	Identity matrix
μ	viscosity of fluid
μ^*	Apparent viscosity
μ_1	viscosity of fluid 1
μ_2	viscosity of fluid 2
ϕ	Solid volume fraction
Ψ	Microscopic quantity
ψ	Average quantity
ρ	Density

ρ_1 Density of fluid 1

ρ_2 Density of fluid 2

ρ_f Density of fluid

σ Stress tensor

σ_1 Stress in fluid 1

σ_2 Stress in fluid 2

τ Tortuosity of the medium

$\mathbf{n}$ Unit normal vector

$\mathbf{t}$ Unit tangential vector

$\mathbf{u}$ velocity vector

ε Porosity of the material

A Cross sectional area

a Grain packing constant

C Sorting index

d Channel diameter

D_d Modal grain size

g Gravitational acceleration

h free or porous surface

h_0 Characteristic height

h_1 Initial height of the flume

h_2 Final height of the flume

h_A Amplitude of the wave

h_f fracture width

K Intrinsic permeability

k Darcy permeability

K_s Packing correction

L Length of the flume

l_0 Characteristic length

M Arbitrary constant

m Frequency of the wave

m_a Archie cementation exponent

N Arbitrary constant

n Viscosity ratio

P Microscopic pressure

p fluid pressure

p_0 Characteristic pressure

p_g Gas pressure

Q Flux of fluid

q Constant values 1 or 3

S_{gt} Trap gas saturation

S_{or} Residual oil saturation

S_{wi} Irreducible water saturation

T Transpose

U_0 Characteristic velocity

U_{fs} Superficial velocity

U_s Tangential velocity

v Specific discharge

V_0 Characteristic velocity

V_t Total volume

V_v Volume of void

w Fracture aperture

x Horizontal Cartesian coordinate

y Vertical Cartesian coordinate

Subscripts

ρ Density

f fluid

fs Superficial

gt Trapped gas

i Fluid phase

or residual oil

t total

v void

wi Irreducible water

Acronyms

D Darcy

DB Darcy Brinkman

LHS Left hand side

LTF Liquid thin film

NS Navier Stokes

PDE Partial differential equation

REV Representative elementary volume

RHS Right hand side

Dimensionless numbers

B_o Bond number

C_a Capillary number

F_r Froude number

R_e Reynolds number

B Ratio of Reynolds to Froude number

Chapter 1

Introduction

1.1 Background and motivation

Understanding the physics of thin films or in other words, studying liquid/liquid interface and gas-liquid (open space) /solid interfaces separately, will open a new avenue into this research since both topics are rich enough to be challenging on their own merits. The term "new avenue" highlights the idea of using the rich insights from interfacial science to completely rethink thin-film challenges. By doing this, we might discover fundamental principles that have been missed in the past, mainly because of the intricate nature of coupled interfaces. This fresh perspective could pave the way for innovative theories, applications, and technologies that push beyond the usual limits of thin-film research. Thin films hold importance across various fields, including biophysics, physics, engineering, and even in natural environments[112]. They are just a few nanometers and a few millimeters thick, and even thicker liquid layers can be found used in various applications, such as environmental cleanup and disease detection diagnostics. Understanding how thin films behave in porous media and at fluid-phase interfaces is crucial for optimizing processes; significantly better design technology can be systematically developed to tackle the complex phenomena that

have been identified.[71, 90].

Porous media are made up of materials that have interconnected void spaces or pores, and they are commonly found in both natural and engineered systems like filters, membranes, rocks, and soils. The structure of these porous materials plays a crucial role in how fluids move through them, impacting processes such as filtration, adsorption, catalysis, diffusion, and capillary rise [82, 141]. When thin films are introduced to porous media, they create additional challenges by changing the fluid distribution, surface interactions, and transport properties of the porous structure.

In single-fluid systems, examining thin films in porous media focuses on how a thin liquid layer interacts with the porous structure. This interaction affects various factors, including mass transport, flow patterns, and wetting behavior. The presence of thin films in porous media can result in phenomena such as film pinning [96], imbibition [131], and pore-scale instabilities [109], which are significant for fields like soil science, chemical engineering, and environmental remediation.

In two-fluid systems, the dynamics of thin films in porous media become more intricate due to the interaction between two immiscible fluids within the porous structure [121]. The behavior of thin films at the interface between the two fluids is crucial for controlling phase distribution, displacement mechanisms, and multiphase flow patterns in porous media. Grasping the interfacial dynamics between the two fluids and their interaction with the porous structure is vital for optimizing processes in fields such as enhanced oil recovery, contaminant transport, and bioremediation [28, 84].

The interface that separates single-fluid and two-fluid systems in porous media offers intriguing research opportunities to explore the complex interactions between various fluid phases and their effects on thin film behavior. By examining how thin films spread at these interfaces, researchers can gain insights into the mechanisms that drive multiphase flow phenomena, interfacial dynamics, and transport processes in porous media environments.

This research thesis dives into the behaviour of thin films in porous media, specifically looking at both single-fluid and two-fluid systems while paying close attention to interfacial dynamics. By blending theoretical modeling with numerical simulations, the study aims to reveal the core principles that govern thin films within porous structures. The results will enhance our understanding of multiphase flow, interfacial phenomena, and transport processes, providing valuable insights for both scientific and engineering applications.

By shedding light on these dynamics, this work can help steer the development of more efficient, sustainable, and safer technologies across various industries.

In short, exploring thin films in porous media, particularly at fluid interfaces presents a complex yet highly significant research area with wide-ranging implications for both fundamental science and practical engineering solutions.

1.2 Thin liquid film and porous media

A thin liquid film is a layer of liquid with a thickness varying from a range of a few nanometers to several micrometers. The thin liquid film can form on solid surfaces, at the interface between two immiscible liquids, or even as free-standing films in the air. Thin liquid films are common in our day-to-day activities in various scientific and industrial processes [10, 85]. A ubiquitous example of thin film is soap bubbles and foams, where a thin layer of liquid encloses a volume of gas bubbles as shown in Figure(1.1). The characteristics and properties of thin liquid film include thickness, capillary force, surface tension, disjoining pressure, etc.

1.2.1 Porous media

A porous medium consists of a solid matrix that remains intact, along with void spaces or pores that can be occupied by one or more fluids, such as water, oil, or gas[2]. Common examples of porous media include soil, rocks, biological tissues, filters, and catalysts, as

Figure 1.1: A classic example of thin liquid films (Source: https://www.pngegg.com/en/png-bzpbx)

illustrated in Figure 1.2.

1.2.2 Single-fluid system with an interface

A single fluid with an interface refers to a system in which a single type of fluid exists in multiple phases (such as liquid and gas) or different states, with a different boundary or interface separating these phases or states [17, 19, 99]. This interface is where the fluid undergoes abrupt changes in properties, such as density, temperature, or pressure, and where important physical processes, like phase transitions, mass, and energy transfer, occur. Despite different phases, the fluid maintains the same chemical composition throughout the system.

1.2.3 Two-fluid system with an interface

A two-fluid system with an interface refers to a physical system in which two distinct fluids coexist but do not mix, forming a boundary known as an interface. This interface separates the two fluids and is where significant physical interactions occur, such as surface tension, interfacial forces, and mass or energy transfer. The fluids involved can be in different phases (e.g., liquid-liquid, liquid-gas) or simply immiscible, and the properties and dynamics at the interface are crucial for understanding the behavior of the system [13, 67, 139].

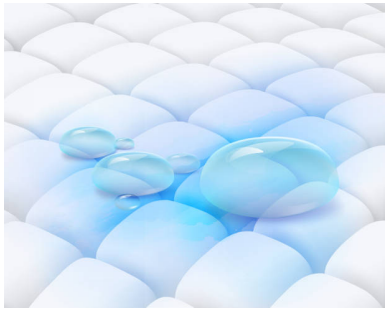

(a) Cotton

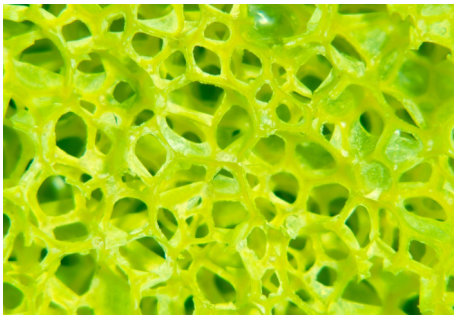

(b) Sponges

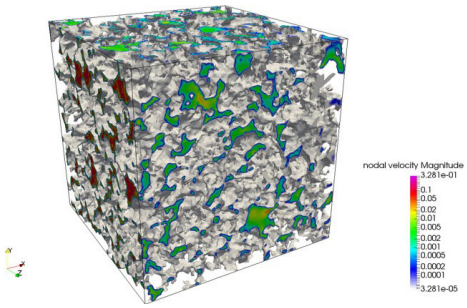

(c) Petroleum reservoir

(d) Stone

Figure 1.2: Examples of porous materials. Source: (https://www.imperial.ac.uk/news/187667/looking-inside-porous-materials-understand-roughness/)

1.3 Aims and objectives

This thesis aims to create and simulate thin film flow models in a porous medium with high porosity, incorporate viscous shear effects, and relate them to the existing ones (models) on a free surface.

These aims will be achieved with the following objectives:

1. Derive lubrication-type model for two-layer thin films separated by an interface.

2. Validate the model in appropriate asymptotic limits, e.g. single-fluid or small alpha.

3. Perform numerical simulations using the Chebfun method and MATLAB as a tool.

In summary, the present research seeks to model and simulate the interaction between thin film flows in free surface and porous media in single and two fluids systems, as given in figure (1.3), and investigate how these interactions between environments affect the dynamics of the fluids, and enhance the efficiency of the recovery of oil and remediation of soil.

In Figure 1.3, we show how the logical transition diagram of various thin film flow models connect with each other under certain asymptotic limits. It features four corner models: two-fluid and single-fluid systems, both in porous (Brinkman-based) and non-porous (Navier-Stokes-based) media. The horizontal transitions illustrate what happens as the medium turns non-porous essentially when the porosity parameter $\alpha \to 0$, the Brinkman equation simplifies to the Navier-Stokes equation. This applies to both single- and two-fluid systems, demonstrating how porous-medium models seamlessly transition to their non-porous equivalents.

On the vertical axis, the transitions depict the scenario where the second fluid becomes insignificant, meaning the viscosity ratio $n = \mu_2/\mu_1 \to 0$. This simplification leads a two-fluid system to act like a single-fluid system in both porous and non-porous environments. The main point here is that these limiting processes are interchangeable: whether we first eliminate the porous effects or simplify the fluid system, we will end up with the same single-

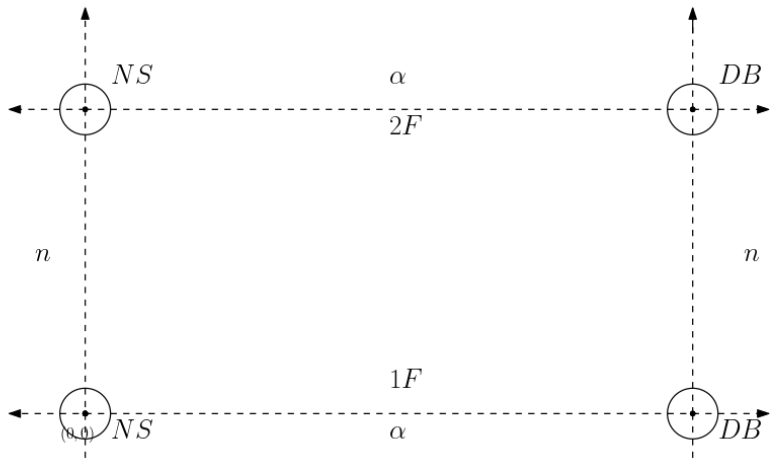

Figure 1.3: Model interaction between thin film in two environments, where NS represents the Navier-Stokes model, DB is Darcy-Brinkman, α is a non-dimensional permeability parameter and n is the viscosity ratio which gives the relationship between two fluids in the system.

fluid, non-porous thin film model governed by the Navier-Stokes equations. This logical framework not only confirms the internal consistency of the models but also offers a clear path for understanding how more complex systems can be simplified into simpler forms. All these above notations and parameters will be discussed in detail in Chapter 3 and 4.

1.4 Thesis Outline

The present thesis comprises 5 chapters, which include the current chapter. In Chapter 2 a comprehensive review of modeling and simulation of the thin film is presented. This consists of the theoretical background and previous derivation of thin film models of single fluid and two fluids in a porous medium, as well as numerical methods and simulations. Darcy's law is discussed in detail along with Brinkman and boundary conditions. Finally, some concepts such as porosity and permeability are discussed.

Chapter 3 presents a derivation of the thin film of a single fluid in porous media using

a Brinkman equation as a momentum equation. Also, it offers a numerical method i.e. Chebfun and numerical solutions. Asymptotic approximation in the limit of α values (zero, infinity) is also discussed.

In Chapter 4 a derivation technique similar to the one in Chapter 3 but using two fluids in porous media, and also consider two fluids in the free surface to see how the two relate with each other.

To the best of our understanding, the derivation of thin film equations for a single fluid in porous media using the Brinkman equation, along with numerical implementation through Chebfun and asymptotic analysis in the limits of $\alpha \to 0$ and $\alpha \to \infty$, as discussed in Chapter 3, has not been tackled in the existing literature. Likewise, Chapter 4 builds on this approach, delving into the more intricate scenario of two-fluid systems in porous media with a consistent derivation framework. The combination of analytical modeling, numerical techniques, and asymptotic analysis for both single- and two-fluid porous media systems seems to offer a fresh perspective that has not been explored in previous studies.

Finally, the conclusions and recommendations of this thesis and potential directions for future work are discussed in Chapter 5.

Chapter 2

Literature review

2.1 Introduction

The research of thin liquid films has fascinated scientists over many decades and focused on its evolution, arising in everyday life ranging from elementary to complicated processes. [20, 100, 140]. Thin films can be composed of common liquids (water), complex materials (polymers), or mixtures of phases and produce a range of interesting behaviours including complex dynamics resulting in regular or chaotic structures, periodic waves, fronts, fingering, and shock phenomena; that pattern formation has captivated many mathematicians, physicists, and engineers to the field of thin films[38].

A thin film flow is a liquid partially confined spatially by a solid (substrate) and partly by a free surface or porous medium where the liquid is in contact with the second (usually gaseous) fluid. The region is given by the thickness h_0, which is much smaller than the characteristic length (usually the wavelength) of the liquid l_0. The flow mainly occurs on a higher scale dimension beneath the action of an external force. A common illustration is the way a thin raindrop flows down a windowpane due to gravity. The velocity u in the direction of the main flow exceeds the velocity v that is perpendicular to the win-

dowpane. According to [112], there exists a unified mathematical theory that leverages the differences in length scales. This theory simplifies the full set of governing equations and boundary conditions into a more manageable, highly nonlinear evolution equation or a series of equations. The long-wave theory, which examines wave behavior in scenarios where the wavelength l_0 is significantly larger than the fluid depth h_0, results in a mathematical framework that, while less complex than the original free-boundary problem, retains many of its key physical characteristics. Furthermore, if the Reynolds number of the flow remains relatively low, one can draw parallels with Reynolds's lubrication theory [123]. Thin film flows have a diverse range of applications in free surface and porous media. Many researchers from fields such as mathematics, biology, biophysics, geophysics, engineering, and medical sciences have highlighted the most significant ones. Studies by [25, 41, 94, 100] have concentrated on analyzing thin film equations, lubrication, wettability, and fluid spreading across substrates. Additionally, research on lining and lung airways, flexible tubes, tear-film flow, and bioadhesion has been conducted by [52, 58, 59, 60, 132]. Optical coatings on lenses and protective coatings are also important areas of study [72, 88, 113]. Other applications include microfluidics, heat exchangers, solar cells, liquid film sensors, and microelectromechanical devices [46, 116, 135, 136, 46]. Furthermore, thin film flows are relevant in understanding mud granular and debris snow avalanches, lava flows, gravity currents, and ice sheet models [5, 11, 56, 65]. In the realm of porous media, applications encompass filtration, energy storage, and conversion [6, 53, 133, 142], as well as catalysis and environmental remediation [43, 55, 73, 149]. Recently, the applications of thin film flow have been reviewed concerning measurement and disturbance wave characteristics [30], the homotopy perturbation method [95], the discrete droplet method [22], and the development and characteristics of coatings [47].

Over the years, many thin film flow models have been developed. One of the most recognized models is the lubrication approximation [8, 12, 21, 39, 115, 130], which simplifies

the set of equations by balancing viscous forces and pressure gradients to govern the flow. The Benney equation, derived from this approximation, differs from simpler thin film models by incorporating higher-order terms [18, 37, 112]. This equation is based on the Navier-Stokes equations using the long-wave approximation. Additionally, the shallow water equations [34, 48, 106] can be derived by integrating the Navier–Stokes equations while assuming that the horizontal length scales are significantly larger than the vertical depth.

A thin-film model that has recently been influenced by numerous theoretical studies is the derivation of the Navier–Stokes [29, 122], Darcy [42, 66, 118], and Brinkman [14, 146] equations in complex geometries or manifolds, which assume a film of constant height. A key similarity among these models is that they lack theoretical solutions, highlighting the necessity for numerical methods to solve the involved PDEs. Various numerical methods have been employed to solve thin-film flow models, including finite difference methods [98, 129], finite volume methods [32, 103], the volume of fluid approach [104, 150], finite element methods [50, 70], meshless methods [23, 117], and spectral methods [57, 89], among others.

In this study, we aim to model a thin film consisting of a single fluid and a two-fluid system with an interface separating them, both in free surface and porous media scenarios. The thin film models for a single fluid and two fluids in a free surface were previously derived by [112] and [75], respectively, using the Navier-Stokes equations as the momentum equation.

The innovative aspect of this work lies in deriving the models for a single fluid and two fluids in porous media, utilizing the Darcy-Brinkman equations as the foundation for momentum. This framework is backed by sophisticated analytical methods, including both linear and nonlinear stability analyses that help identify the thresholds for convective instabilities.

It also employs energy methods to evaluate the bounds of nonlinear stability. Specifically, this study resonates with the approaches taken by [97] who explored stability in porous media flows through perturbation techniques and spectral methods. Moreover, it references exact solutions to the Darcy-Lapwood-Brinkman equation for flows driven by vorticity and

numerical techniques like Chebyshev spectral collocation for tackling eigenvalue problems. Together, these strategies ensure a thorough validation of the models developed, even under varying conditions of gravity, through flow, and interfacial dynamics.

The thin film models were numerically solved using the Chebfun method within a specified domain.

2.2 Concept of porosity and permeability

Key concepts in various scientific and engineering disciplines that describe the properties of porous media include porosity and permeability.

2.2.1 Porosity

Porosity is a measure of the void spaces in a material, expressed as a fraction or percentage of the total volume [14, 78].
Mathematically, it is defined as:

$$\varepsilon = \frac{V_v}{V_t} \tag{2.1}$$

where ε represents the porosity, V_v is the volume of voids (or pores) within the material, and V_t is the total volume of the material, which includes both the solid and void portions. This ratio can vary from nearly 0% in very dense, non-porous materials to almost 100% in highly porous materials like foams. It plays a crucial role in determining a material's ability to hold and transmit fluids. In geological contexts, porosity typically refers to the pore spaces found within rocks and sediments, which can be occupied by fluids such as water, oil, or gas.

Porosity is a key parameter in understanding the microstructures of porous materials [68]. It represents the volume of voids that can hold fluid, in relation to the total volume of the material. The pore system, which can consist of either interconnected or isolated pores and

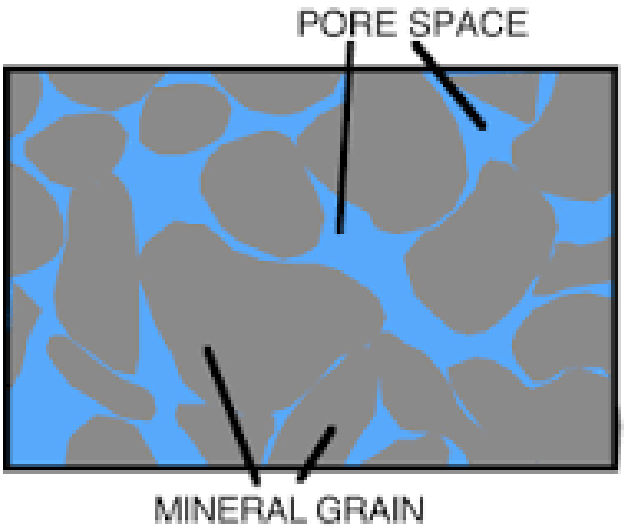

Figure 2.1: Porosity of a rock. Source:(https://home.wgnhs.wisc.edu/water/wisconsin-aquifers/understanding-porosity-density/)

small channels, can be categorized into various classes of porosity. These classifications can be based on accessibility (open, closed, blind, and through pores) [124], shape (cylindrical, funnel, bottle-shaped) [77], and size (micro, meso, and macro pores) [148].

Open porosity refers to the volume of pores that are accessible or interconnected. In contrast, closed porosity pertains to the portion of the pore system made up of isolated pores that do not connect with other pore spaces or the external environment. While this type of porosity does not participate in mass transfer, it does influence the strength of the material. Additionally, the characterization of the pore system can be enhanced by examining the pore size distribution, which indicates the range and relative frequency of different pore sizes within a material.

2.2.2 Permeability

This refers to how well a porous material can allow fluids to flow through its interconnected pore spaces.

Permeability is mathematically defined by Darcy's law, which connects the flow rate of

a fluid through a porous medium to the pressure gradient applied, the fluid's viscosity, and the characteristics of the medium itself and is given as

$$Q = -\frac{kA}{\mu}\frac{dP}{dx}, \tag{2.2}$$

where, Q is the volumetric flow rate (m^3/s), k is the permeability of the medium (m^2), A is the cross-sectional area to flow (m^2) , μ is the dynamic viscosity of the fluid $(Pa \cdot s)$ and $(kg \cdot m^{-1} \cdot s^{-1})$, $\frac{dP}{dx}$ is the pressure gradient (Pa/m). An alternative form using the specific discharge (or Darcy velocity) is given as

$$\mathbf{u} = -\frac{k}{\mu}\frac{dP}{dx}, \tag{2.3}$$

where, $\mathbf{u} = \frac{Q}{A}$ is the Darcy velocity (m/s).

In simpler terms, permeability is influenced by porosity; generally, the greater the porosity, the higher the permeability. However, it also depends on how well the pore spaces are connected, which allows fluid to flow through. The connectivity of these pores is affected by various factors, including the size and shape of the grains, the distribution of grain sizes, and the influence of capillary forces that are linked to the rock's wetting properties. The permeability of rocks can vary widely, ranging from nano-Darcy, 1 nD $= 9.869233 \times 10^{-19}$ m^2 to micro-Darcy, 1 μD $= 9.869233 \times 10^{-19}$ m^2 for granites, shales, and clays that create a compartmentalized reservoir, to several Darcies for high-quality reservoir rocks. Typically, a threshold of $1\mu D$ is used to categorize reservoir rocks, with those below this mark not considered reservoirs unless in special cases, such as a fractured reservoir [102]. For reservoir rocks, permeability can be classified as shown in the Table 2.1

Permeability is assessed in the lab by allowing a fluid with a known viscosity to flow through a core sample of specific dimensions at a controlled rate. This involves measuring the pressure drop across the core or setting the fluid to flow under a fixed pressure difference

Permeability Value (μD)	Classification
< 10	Fair
$10 - 100$	High
$100 - 1000$	Very high
> 1000	Exceptional

Table 2.1: Reservoir permeability classification

and recording the resulting flow rate.

Permeability is influenced by various factors, one of which is the extent to which the available pore space is saturated with the flowing fluid. The pore space may not be fully saturated with a single fluid; it can contain two or more fluids. When both oil and water flow at different rates within the pores, the individual permeabilities of each fluid will differ and will not match the permeability of the rock when only one fluid is present. These permeabilities are affected by the properties of the rock as well as the saturations, distributions, and characteristics of each fluid. When the rock contains only one fluid, its permeability reaches a maximum value known as absolute permeability. In cases where two fluids are present, the permeabilities of both fluids depend on their respective saturations and can be graphed against fluid saturation, as illustrated in Figure 2.2 from [61]. These are referred to as effective permeabilities. Both effective permeabilities are consistently lower than the absolute permeability of the rock, and their combined value is also always less than the absolute permeability. The individual effective permeabilities are frequently expressed as a fraction of the rock's absolute permeability when either of the two fluids is at 100 percent saturation, and these are termed relative permeabilities.

In Figure 2.2, the effective and relative permeability of a fluid decreases as its saturation drops, and there is a minimum saturation level that must be reached for the fluid to flow. For oil, it remains immobile until its saturation reaches about 20 per cent, which is referred to as the residual oil saturation, S_{or} [1]. Similarly, water has an immobile fraction known as the irreducible water saturation, S_{wi}, while gas has a trapped gas saturation, S_{gt}.

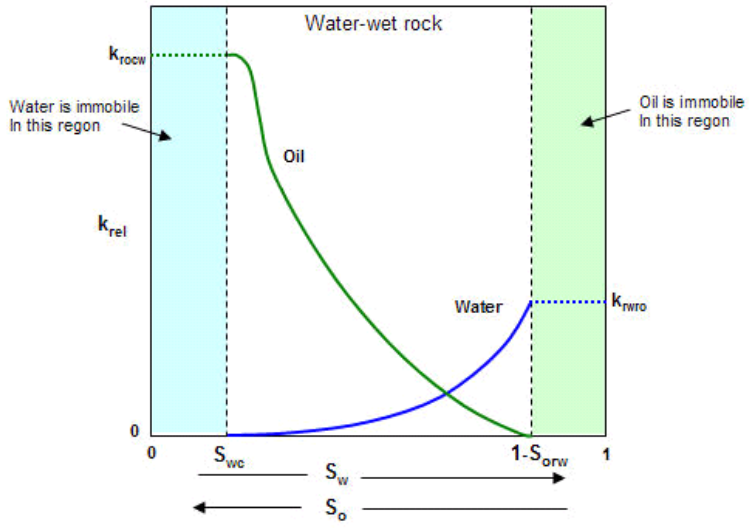

Figure 2.2: Relative Permeability Curves (Oil and Water). Source: https://www.ihsenergy/reference material/general concepts/relative permeability.htm

On the graph, there is a point where the curve intersects, indicating that the permeability for each fluid is equal, ensuring both can be produced with equal simplicity. As oil saturation rises, the permeability to oil increases while that to water decreases, and the opposite is also true. Therefore, in oil reservoirs, it is crucial to minimize water production, as it not only fails to generate revenue but also reduces the reservoir's permeability to oil, making extraction more challenging.

2.2.3 PoroPerm Relationships

Permeability and porosity are two key properties that influence how fluids move and are stored in porous materials [134]. While there is a direct relationship between the two, it is not strictly proportional. Increased porosity can enhance permeability since more pore space may facilitate greater fluid flow. However, this isn't always true; permeability also relies on the connectivity of the pores, not just their volume. A material can exhibit high porosity but low permeability if the pores are poorly interconnected, as seen in some aquifers. Within

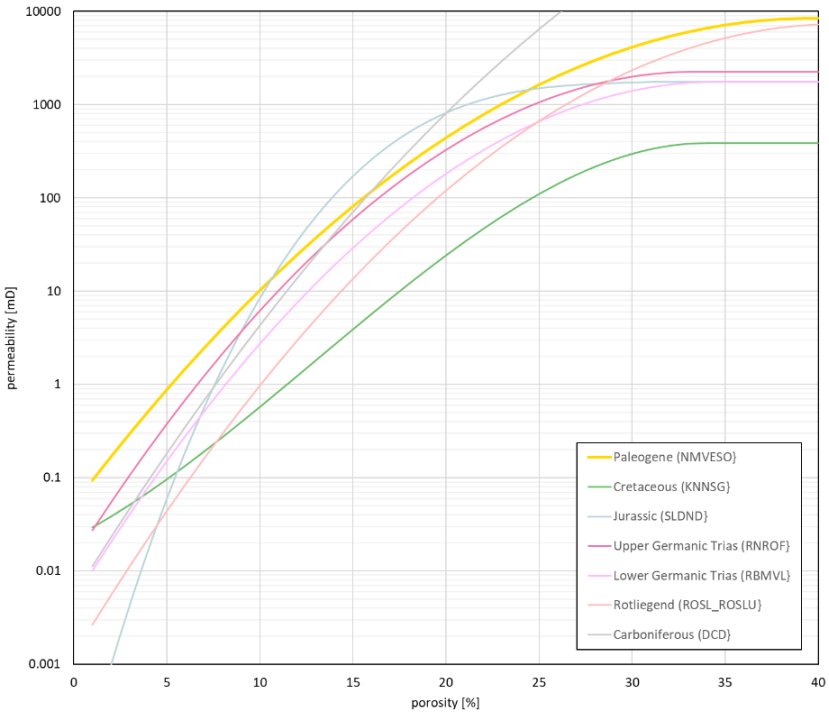

Figure 2.3: Porosity Permeability relations for selected aquifers. Source: https://www.thermogis.nl/en/porosity-and-permeability

a lithostratigraphic group, the relationships may vary slightly for each aquifer, as illustrated in Figure 2.3.

A lithostratigraphic unit is a volume of rock that is defined and distinguished from other units based on its lithologic (rock) characteristics, such as composition, grain size, colour, texture, or sedimentary structures.

The intricate relationship between permeability and pore geometry has led to extensive research. Several fundamental laws and models have been established to connect the two. The most widely recognized is the Kozeny-Carman equation. We also have a wide range of empirical approximations for calculating permeability, with some examples provided in Table 2.2.

In this context, k represents permeability, d denotes the channel diameter, h indicates the fracture width, w refers to the fracture aperture, ϕ stands for porosity, D_d is the modal

Name	Equation
Solution Channel	$k = 0.2 \times 10^8 \times d^2$
Fractures	$k = \frac{0.544 \times 10^8 \times w^3}{h}$
Berg equation	$k = 8.4 \times 10^{-2} \times d^2 \phi^{5.1}$
Van Baaren equation	$k = 10 \times D_d^2 \phi^{(3.64+m)} C^{-3.64}$
Wyllie and Rose equations	$k = \left[\frac{100\phi^{2.25}}{S_{wi}}\right]^2$
Timur equation	$k = \frac{0.136\phi^{4.4}}{S_{wi}^2}$
Morris and Biggs equation	$k = \frac{C\phi^3}{S_{wi}^2}$
Slichter equation	$k = \frac{10.2d^2}{K_s}$
Kozeny-Carman equation	$k = \frac{cd^2\phi^3}{(1-\phi)^2}$
RGPZ equation	$k = \frac{1000d^2\phi^{3m}}{4am^2}$

Table 2.2: Permeability relationships, Source: [7]

grain size, C is the sorting index, S_{wi} signifies irreducible water saturation, K_s is the packing correction, c is a constant, m is the Archie cementation exponent, and a is a grain packing constant. This study examines hetero permeability in relation to the Kazeny-Carman equation.

$$k(y) = \frac{cd^2\phi^3(y)}{(1-\phi(y))^2} \tag{2.4}$$

where, $k(y)$ and $\phi(y)$ are permeability and porosity that depend on y, and y is a spatial variable representing vertical position or depth in a porous material. In this section, we will explore the relevant studies on fluid flow in porous media, with a focus on Darcy's law, its limitations, Brinkman's contributions (Extended Darcy's law), and the impact of boundary conditions.

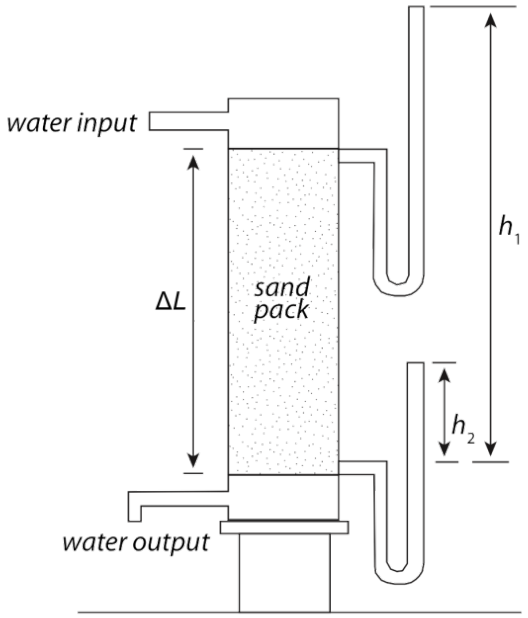

Figure 2.4: Schematic of Darcy's original experimental apparatus. Source- https://serc.carleton.edu/integrate/teaching materials/water science society/student materials/926

2.2.4 Darcy's law

In the mid-nineteenth century, a French hydraulic engineer named Henry Darcy worked on enhancing and modernizing the fountain of Dijon [91]. He created a vertical experimental tank filled with sand, where water was injected from the top and allowed to flow out from the bottom. Through this setup, he conducted experiments on unidirectional flow in vertical, homogeneous, randomly, and loosely packed sand filter beds, as illustrated in Figure 2.4. From the experiments, data was collected on the length of the flume (ΔL), the cross-sectional area of the flume (A), the height difference ($h_2 - h_1$), and the water flux (Q) both with and without granular (filtering) material in the flume. The flux measurements were then plotted, normalized by the area, against the ratio of the height difference to the length of the flume.

Darcy also noted that in a steady-state flow through a specific porous medium, there exists a linear relationship between the water flux and the applied pressure drop. This

relationship is influenced by the hydraulic conductivity coefficient k. This principle is known as Darcy's law.

$$Q = -\frac{kA(h_2 - h_1)}{\Delta L} \tag{2.5}$$

The equation describes a volumetric flow rate, denoted as Q. The negative sign signifies that the fluid moves down the hydraulic gradient, transitioning from areas of higher values to those of lower values. The hydraulic conduction coefficient k, often referred to as permeability in equation (2.5), can also be viewed as a measure of flow resistance through porous media. This coefficient is considered constant and is determined by the characteristics of the porous medium. In the case of packed beds or fibers, another way to express the resistance of the medium is through a dimensionless parameter known as the friction factor [7]. Dimensional analysis leads to the following relationship:

$$k = \frac{\rho g K}{\mu} \tag{2.6}$$

where g represents gravitational acceleration, μ is the dynamic viscosity, and k denotes the intrinsic permeability of a specific sand pack and K represent hydraulic conductivity in terms of k.

The specific discharge $v = \frac{Q}{A}$, also known as Darcy flux, indicates the volume of fluid that flows through a given area of the porous medium, and it is typically referred to as a velocity. According to [91], since only a portion of the cross-sectional area is available for flow (with most of the area obstructed by sand grains), v does not represent velocity in the microscopic sense. Rather, v reflects the apparent macroscopic velocity, which is derived from averaging the microscopic fluxes within representative elementary volumes (REVs). Consequently, the macroscopic fluid velocity, defined as the volume of fluid flowing per area occupied by fluid, is expressed as $\frac{v}{\varepsilon}$, where ε denotes the porosity associated with the REV.

Darcy's law in terms of specific discharge or Darcy velocity is first proposed mathemati-

cally by [107] and [147] and is given by,

$$\mathbf{u} = -\frac{K}{\mu}(\nabla p - g\rho\nabla y), \tag{2.7}$$

where p is the fluid pressure and y is the vertical coordinate. The equation (2.7) expressed conservation of momentum and was derived from the Navier–Stokes equations by averaging and neglecting inertial and viscous effects by [64] and later for Stokes flow by [144]. We noticed that Darcy's law (2.7) is related to Fourier's law for heat conduction [35], Fick's law for fluid concentrations in diffusion theory [151], and, Ohm's law in the field of electrical networks [36]. It also assumes that a reversible fluid process is a special case of the more general physical laws of irreversible processes first described by [110].

The Continuum Approach

The continuum approach of Darcy's Law offers valuable insights for modeling and simulating fluid flow through porous media by averaging the effects of the intricate pore structure. Due to the complexity of typical porous media, numerical simulations often rely on simplified boundary conditions or conceptual continuum models, allowing for the analysis of flow behavior on a larger (average) scale using spatially averaged Navier-Stokes equations [26, 146]. Given these considerations, the continuum approach is generally the more appropriate choice. This method is typically implemented through either statistical averaging or spatial averaging techniques. However, both methods produce equivalent flow quantities when the spatially averaged relationships are of primary interest [105].

The spatial averaging method provides averaged flow quantities over a representative elementary volume (REV) that is significantly larger than the scales of the pore space and the solid matrix of the porous medium. The average obtained remains independent of the size of the volume element. For example, in a single-phase flow through porous media, the

total volume of a REV is the sum of the volume occupied by the fluid and that occupied by the solid matrix. Microscopic scales (pore sizes) are typically represented by lowercase letters, while averaged flow quantities are denoted in uppercase. For instance, microscopic and averaged pressures are represented as p and P, respectively.

Using spatial averaging in porous medium flow, the microscopic flow quantities within a finite microscopic elemental volume can be connected to their corresponding averaged quantities in a defined Representative Elementary Volume (REV) through a superficial averaging method [7]. This process yields a quantity Ψ_{fs}, which is derived by averaging the respective microscopic quantity ψ across the entire elemental volume composed of both fluid and solid components. The velocity obtained through this method is referred to as the 'superficial velocity $\mathbf{u}$'. Intrinsic averaging represents a second type of spatial averaging, which involves averaging all microscopic quantities solely over the fluid volume of the elemental volume. The velocity derived from this approach is known as intrinsic velocity.

Using the continuum approach for steady-state fluid flow with fluid density ρ_f, we can derive the differential equations related to the continuity equation and the averaged momentum equations [145]. These equations can be solved numerically with suitable boundary conditions, independent of the chosen REV model. The results can then be validated using the empirical Darcy Law, which serves as the constitutive equation applicable at sufficiently low flow rates, assuming that body forces in the flow are negligible [9]. The Darcy Law similar to (2.3) can be expressed as [7]

$$\mathbf{u} = -\frac{1}{\mu} K_T (\nabla p) \tag{2.8}$$

where μ represents the fluid dynamic viscosity, K_T is a second-order permeability tensor, and ∇p is the pressure gradient applied across the porous medium. In an isotropic medium, the permeability is scalar, allowing us to replace the tensor K_T with k, known as the Darcy

permeability. While Darcy's law is a key principle in fluid dynamics for describing fluid flow in porous media, it doesn't encompass all the practical aspects of such flow. There are notable limitations to its application. The primary limitation is that it overlooks inertial forces in comparison to viscous forces and assumes that the flow through porous media is laminar. To overcome these limitations, various extensions and modifications have been proposed, one of which is Brinkman's law. The Brinkman equation, introduced by H.C. Brinkman in 1947, represents an important advancement of Darcy's Law. It tackles some of the shortcomings of Darcy's Law, particularly in situations where it fails to adequately describe fluid flow in porous media. Additionally, it enhances Darcy's Law by incorporating a term that accounts for the viscous shear stress within the fluid. This contribution is vital for connecting Darcy's Law, which is applicable to low-velocity, laminar flow in porous media, with the Navier-Stokes equations, which govern viscous flow in free space.

The Brinkman equation is typically applied in scenarios where fluid flow is characterized by higher Reynolds numbers or when the medium's porosity is relatively low. It is expressed as

$$\frac{\mu}{k}\mathbf{u} = \mu^*\nabla^2\mathbf{u} - \nabla p, \tag{2.9}$$

where μ^* represents an apparent (Brinkman) viscosity, a parameter influenced by both the fluid and the geometry and structure of the porous medium [7]. Consequently, Brinkman utilized (2.9) along with various boundary conditions to address the entire flow domain and to compare the outcomes with an empirical relationship proposed by [27]. It was observed that for solid particles with a volume fraction $\phi < 0.6$, there was a good correlation with Carman's experimental findings when the apparent viscosity μ^* in the Brinkman equation matched the fluid's dynamic viscosity μ. In this context, the selected value of μ^* is referred to as an effective viscosity [4].

Many researchers have confirmed the validity of the Brinkman equation for high porosity,

including [33, 49, 62, 63, 125, 138]. However, most studies involving low porosity have shown that the Brinkman equation consistently fails to accurately predict the flow field, as noted in [40, 69, 86, 87]. Additionally, [79] found that the Brinkman model tends to underestimate the flow resistance at the interface. Consequently, boundary effects warrant further investigation into the porous medium. The Brinkman equation has been further validated through experimental studies, although some of the findings have sparked controversy. Certain theoretical predictions regarding the flow in highly porous media, based on the Brinkman equation, have aligned with experimental data [93, 80]. However, [45] contended that the permeabilities used are single scalar values that do not accurately represent general flow, suggesting that the empirical correlations observed in those experiments do not necessarily confirm the validity of the Brinkman equation for high porosity media. To support their claim, they presented fundamental solutions for creeping flow through porous media and, upon comparing their results with those derived from the Brinkman equation, concluded that for $1 - \varepsilon > 0.05$, the Brinkman solution loses its predictive capability, although it still serves as a useful qualitative tool. Additionally, [54] compared velocity measurements with analytical data for $\varepsilon = 0.028$ and determined an apparent viscosity of $\mu^* = 7.5\mu$. Overall, all studies indicate that there is a specific valid form of the Brinkman equation applicable to low porosity [105, 125].

In an effort to study the modeling of the apparent viscosity in the Brinkman equation, researchers have produced a variety of results. [81] examined the flow at the interface between free surfaces and porous media. They calculated the energy dissipated in the flow around isolated spheres and discovered that the apparent viscosity from the equation is lower than the fluid viscosity, meaning $\mu^* < \mu$. This finding contrasts with the results from [93], indicating that outcomes can vary. Later, [80] utilized dilution theory to address the Stokes equation for flow through a random arrangement of fixed spheres, with ε values ranging from 0.3 to 0.5. In this context, it was assumed that the viscosity is lower than Brinkman's viscosity,

meaning $\mu < \mu^*$, which contrasts with the findings of [81]. A numerical investigation into the flow at the surface of porous media was also conducted by [86, 87], who developed their porous media model using rectangular and hexagonal arrays of cylindrical shapes. They concluded that when the fluid flow is perpendicular to the cylinders, Brinkman's viscosity is less than the fluid's viscosity ($\mu^* < \mu$). Conversely, if the flow aligns with the cylinders, the fluid's viscosity is lower than Brinkman's viscosity ($\mu < \mu^*$). Additionally, [15] employed a volume-averaging method to demonstrate that

$$\frac{\mu^*}{\mu} = \frac{\tau}{1-\varepsilon},$$

where τ represents the tortuosity of the medium. Similarly, [108] presented different findings that

$$\frac{\mu^*}{\mu} = \frac{1}{1-\varepsilon}.$$

However, Ochoa also addressed some concerns regarding this apparent viscosity. Given the ambiguity surrounding the Brinkman viscosity concept and the mixed results found in the literature, [79] suggested adopting a variable apparent viscosity model.

2.2.5 Boundary Conditions Contributions

One way to address the issue of flow through porous media involves establishing boundary conditions at the interface between the fluids. Numerous researchers have made contributions to these boundary conditions, utilizing both empirical and analytical approaches.

The initial experimental investigations into the interfacial boundary conditions for Poiseuille flow through and over a porous medium were carried out by [16], who identified a tangential slip velocity u_s at the interfaces of the porous media. [127] later formulated an equation describing flow through an inhomogeneous porous medium, where porosity and permeability exhibit a sharp discontinuity, transitioning from reservoir-scale values to fracture-dominated

flow (effectively infinite permeability and near-unit porosity).

In another research study, [101] tackled the issue of interfacial boundary conditions. They proposed maintaining continuity in both the velocity and the velocity gradient (a spatial derivative of the velocity field across the interface between a free-flow region), by incorporating the Brinkman term into the momentum equation for the porous side. [86, 87] conducted a numerical analysis of the microscopic flow near the surface of a two-dimensional porous medium composed of simple arrays of cylindrical inclusions. They employed the boundary-integral method to address the Stokes flow in scenarios where the idealized porous medium was aligned with and across the flow.

Additionally,[108] introduced a jump momentum transfer condition at the interface between the fluids in a porous medium. This approach relies on the volume-averaged momentum equation derived from Darcy's law combined with the Brinkman equation to address both free flow and porous media scenarios.

More recently, [31] examined the flow dynamics of free and porous media to establish the boundary condition applicable at the interface. By aligning asymptotic expansions with a heterogeneous transition layer at the boundary, they developed a model where the condition is determined by fluid stress.

Chapter 3

Single fluid with an interface

Single fluid with an interface between liquid and gas refers to a system where a homogeneous fluid (such as water) exists as shown in Figure 3.1.

3.1 Thin film in a porous medium

In this subsection, we shall derive the thin film models used to describe the behavior of fluids in a porous medium and later show that it exhibits an interesting connection with free surface media, especially when a given parameter say α is small, which is defined in terms of a permeability of a porous material. When the parameter, α of the porous medium is very small, a simple convergence occurs between the thin film models for porous media and free surface media. In the case of a very small value of alpha, the flow through the porous medium becomes dominated by the large, interconnected pathways, resembling the behaviors of free surface flows where fluid movement is more open and unconstrained. The effect of the small α of the porous medium allows fluids to flow more freely and quickly through the system, reducing the influence of the pore-scale interaction and enhancing the dominance of macroscopic flow behavior. The convergence of thin film models for porous media and

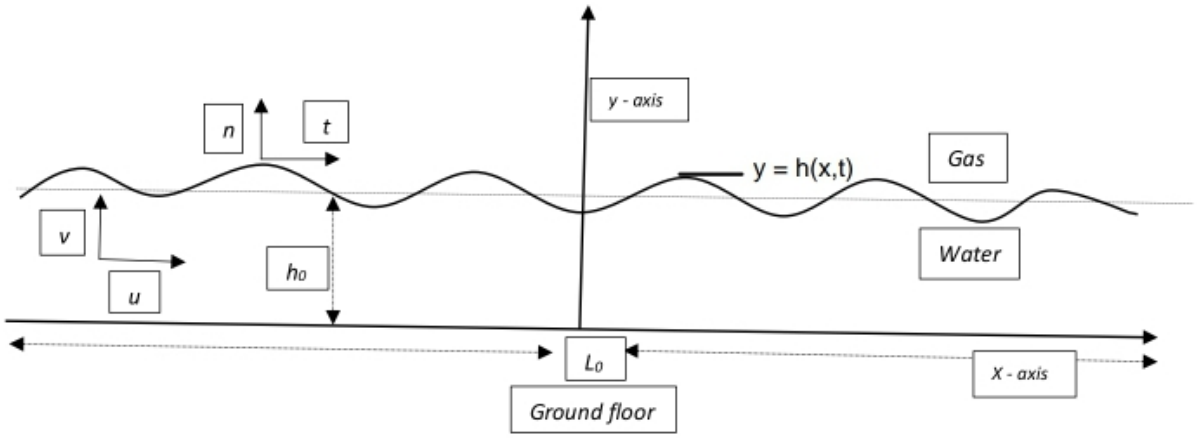

Figure 3.1: Sketch of water-gas flow with a sharp separating interface. The horizontal and vertical velocities are given as u and v, and the characteristic length and height are given as L_0 and h_0 and $y = h(x,t)$ is the interface between the fluids

free surface media under conditions of a value of $\alpha = 0$, provides valuable insight into the behavior of fluids in diverse environments. Researchers can leverage this relationship to gain a deeper understanding of fluid dynamics, optimize modeling approaches, and explore the interplay between porous structures and surface flows in natural and engineering systems. Finally, we show the relationship between thin film for porous media and free surface media, and this showcases how different fluid dynamic scenarios can exhibit similarities and overlap under specific conditions.

3.1.1 Governing Equations

Let's consider the two-dimensional plane, the following parameters in the equations governing the flow of the fluids in any region are to be considered; $\mathbf{u} = (u, v)$, where, u, v are velocities of the fluid in horizontal and vertical components. Also ρ, μ, and p are the density, viscosity, and pressure of the fluid respectively. The creeping flow in the free flow region is characterized

by the continuity equation, which comes from mass balance, along with the incompressible Stokes equations. These equations simplify the Navier-Stokes equations (NS) for low fluid velocities, where inertial forces are minimal compared to viscous forces, allowing us to neglect the convective non-linear term $(\mathbf{u} \cdot \nabla)\mathbf{u}$ [51], and is given by

$$\nabla \cdot \mathbf{u} = 0, \quad \mu \nabla^2 \mathbf{u} = \nabla p + \rho \mathbf{g}, \tag{3.1}$$

where $\nabla^2 = \dfrac{\partial^2}{\partial x^2} + \dfrac{\partial^2}{\partial y^2}$, $\mathbf{g} = (0, -g)$ is a force of gravity, and x, y are Cartesian coordinates. For an incompressible and viscous flow in porous media, as described by the Darcy equation (D), where inertial effects are negligible. [92, 51], and is given by

$$\nabla \cdot \mathbf{u} = 0, \quad \mathbf{u} = -\frac{k}{\mu} \nabla p + \rho \mathbf{g}, \tag{3.2}$$

where k is the permeability of a porous material.

Brinkman's extension of Darcy's law is both mathematically and physically more suitable than Darcy's law when considering boundary layer effects or the high porosity of the porous medium. Unlike Darcy's law, the Darcy Brinkman equation (DB) is fully compatible with the presence of boundary layer regions, allowing it to effectively capture and model these effects within the porous medium and is given by

$$\nabla \cdot \mathbf{u} = 0, \quad \mu^* \nabla^2 \mathbf{u} - \frac{\mu}{k} \mathbf{u} = \nabla p + \rho \mathbf{g}, \tag{3.3}$$

where μ^* represents the effective viscosity of the fluid, which is influenced by the characteristics of the porous material. According to [7], there was a good match with Carman's experimental relation when the effective viscosity μ^* was set equal to the dynamic viscosity of the fluid, μ. This selection of μ^* is commonly referred to as the Brinkman model.[4] However, it is generally assumed that in creeping flow conditions $\mu = \mu^*$. The Continuity

equation and equation (3.3) can be expressed as follows.

$$\frac{\partial u}{\partial x} + \frac{\partial v}{\partial y} = 0 \tag{3.4}$$

and

$$\mu \left(\frac{\partial^2}{\partial x^2} + \frac{\partial^2}{\partial y^2} - \frac{1}{k} \right) u = \frac{\partial p}{\partial x} \tag{3.5a}$$

$$\mu \left(\frac{\partial^2}{\partial x^2} + \frac{\partial^2}{\partial y^2} - \frac{1}{k} \right) v = \frac{\partial p}{\partial y} + \rho g \tag{3.5b}$$

3.1.2 Boundary Conditions

The boundary conditions for viscous, incompressible liquids require sticking to the floor [139], so that water velocities u and v are equal to the wall velocities, respectively are given as,

$$u = 0 \quad \text{(no slip)} \quad \text{and} \quad v = 0 \quad \text{(no penetration) conditions.} \tag{3.6}$$

3.1.3 Interface Condition

The condition at the interface can be simply achieved when it is a single-valued function at $y = h(x, t)$ and this can result in the following equations:

$$v = \frac{\partial h}{\partial t} + u \frac{\partial h}{\partial x}. \tag{3.7}$$

and

$$\mathbf{n} \cdot (\boldsymbol{\sigma} \cdot \mathbf{n}) = \gamma \kappa, \quad \mathbf{t} \cdot (\boldsymbol{\sigma} \cdot \mathbf{n}) = 0. \tag{3.8}$$

Equation (3.7) represents the kinematic boundary condition, which ensures that the speed of the interface is balanced with the normal component of the water velocity at that interface[112]. Additionally, equations (3.8) describe the normal and tangential stress conditions, where σ

denotes the stress tensor of the water, $\mathbf{n}$ is a unit vector normal to the interface, $\mathbf{t}$ is a unit vector tangential to the interface, γ represents the surface tension coefficient, and κ indicates the curvature of the interface. The stress tensor $\boldsymbol{\sigma}$ is defined as follows.

$$\boldsymbol{\sigma} = -p\mathbb{I} + \mu\left[\nabla u + \nabla u^T\right]. \tag{3.9}$$

where $\mathbb{I}$ is a unit matrix. The unit normal $\mathbf{n}$, unit tangent $\mathbf{t}$, and the curvature κ of the interface are given respectively by the equations [112, 114]

$$\mathbf{n} = \frac{\left(-\frac{\partial h}{\partial x}, 1\right)}{\sqrt{1+\left(\frac{\partial h}{\partial x}\right)^2}}, \quad \mathbf{t} = \frac{\left(1, \frac{\partial h}{\partial x}\right)}{\sqrt{1+\left(\frac{\partial h}{\partial x}\right)^2}}, \quad \text{and} \quad \kappa = \frac{\frac{\partial^2 h}{\partial x^2}}{\sqrt{\left(1+\left(\frac{\partial h}{\partial x}\right)^2\right)^3}}. \tag{3.10}$$

Also the normal and the tangential shear stress on $y = h(x,t)$ are given by the equations.[112, 126]

$$\frac{\gamma\frac{\partial^2 h}{\partial x^2}}{\sqrt{\left(1+\left(\frac{\partial h}{\partial x}\right)^2\right)^3}} - \frac{2\mu}{1+\left(\frac{\partial h}{\partial x}\right)^2}\left[\frac{\partial h}{\partial x}\left(\frac{\partial u}{\partial y}+\frac{\partial v}{\partial x}\right) - \left(\frac{\partial h}{\partial x}\right)^2\frac{\partial u}{\partial x} + \frac{\partial v}{\partial y}\right] + p - p_g = 0 \tag{3.11}$$

and

$$2\frac{\partial h}{\partial x}\left(\frac{\partial v}{\partial y}-\frac{\partial u}{\partial x}\right) + \left[1-\left(\frac{\partial h}{\partial x}\right)^2\right]\left[\frac{\partial u}{\partial y}-\frac{\partial v}{\partial x}\right] = 0, \tag{3.12}$$

where p_g is the pressure exerted on the gas phase, which can be set to be zero without loss of generality.

3.1.4 Non-dimensionalisation

We introduce the dimensionless asterisked coordinates, velocities, and pressure as

$$x^* = \frac{x}{L_0}, \quad y^* = \frac{y}{h_0}, \quad h^* = \frac{h}{h_0}, \quad u^* = \frac{u}{U_0}, \quad v^* = \frac{v}{V_0}, \quad \text{and} \quad p^* = \frac{p}{P_0}, \tag{3.13}$$

where L_0, h_0, P_0, and U_0, V_0 are characteristic length, height, pressure and velocities in x, $y-$direction. In this dimensionless variable, the continuity equation is rewritten as

$$\frac{\partial u^*}{\partial x^*} + \frac{V_0}{U_0}\frac{L_0}{h_0}\frac{\partial v^*}{\partial y^*} = 0. \tag{3.14}$$

For the coefficient of the dimensionless continuity equation to be unity, we choose the characteristic lengths and velocities as

$$\frac{V_0}{U_0}\frac{L_0}{h_0} = 1, \tag{3.15}$$

and defined characteristic pressure as

$$P_0 = \frac{\mu L_0 U_0}{h_0^2}. \tag{3.16}$$

With these definitions of the characteristic velocities and pressure, the horizontal and vertical components of (DB) in (3.3) in Cartesian coordinates can be written

$$\frac{\partial p^*}{\partial x^*} = \left(\epsilon^2 \frac{\partial^2}{\partial x^{*2}} + \frac{\partial^2}{\partial y^{*2}} - \alpha^2\right) u^*, \tag{3.17}$$

$$\frac{\partial p^*}{\partial y^*} = \epsilon^2 \left(\epsilon^2 \frac{\partial^2}{\partial x^{*2}} + \frac{\partial^2}{\partial y^{*2}} - \alpha^2\right) v^* - \tilde{B}, \tag{3.18}$$

where, $\epsilon = \dfrac{h_0}{L_0}$ is a height-to-length ratio, $\alpha = \dfrac{h_0}{\sqrt{k}}$ is a dimensionless parameter defined in terms of k, the permeability parameter, $\tilde{B} = \epsilon B$, and B is a number defined by $\dfrac{\rho h_0^2}{\mu U_0} g$, where

it represents the effect of gravity at the leading order.

The normal and tangential equations (3.11) and (3.12) when writing in non-dimensional variables according to scale (3.13) are ,

$$\frac{1}{\tilde{C}}\frac{\partial^2 h^*}{\partial x^{*2}} = 2\epsilon^2\left[\frac{\partial u^*}{\partial x^*} - \frac{\partial h^*}{\partial x^*}\left(\frac{\partial u^*}{\partial y^*}\right)\right] - p^*, \quad \text{at} \quad y = h(x,t), \tag{3.19}$$

where $\tilde{C} = \dfrac{C}{\epsilon^3}$ and C is a capillary number defined by $C = \dfrac{\mu U_0}{\gamma}$, as in [112], where it retains surface tension effect at the leading order, and

$$2\epsilon^2\frac{\partial h^*}{\partial x^*}\left[\frac{\partial v^*}{\partial y^*} - \frac{\partial u^*}{\partial x^*}\right] + \left[\frac{\partial u^*}{\partial y^*} - \epsilon^2\frac{\partial v^*}{\partial x^*}\right] = 0, \quad \text{at} \quad y = h(x,t). \tag{3.20}$$

3.1.5 Lubrication Theory

We introduce the assumption of a parameter $\epsilon = \frac{h_0}{L_0} \ll 1$, known as "lubrication parameter" and is taking asymptotically small as to the derived reduced set of equations in the lubrication [38], where h_0 and L_0 are characteristic lengths of the confined fluid to the thin gap $0 < y \ll h(x,t)$ [3]. Recently lubrication theory was successfully applied to the modeling of the evolution of a thin liquid film, this is the work of [38, 112]. For two-layer thin films with no-slip conditions at the interfaces, the derivation of lubrication equations is done by [37, 83, 120]. In this case a film of fluid between nearly parallel surfaces of which the radii of curvature are larger when compared with the thickness of the film [123]. We let x be a distance measured on the surface in the direction of relative motion, and y to be a distance measured everywhere perpendicular to the surface. Since the surfaces are nearly parallel and they remain in the initial direction, the velocity v in the y-direction will be much smaller than the velocity u in the x-direction. For simplicity, the asterisk (*) in the above will be omitted.

For the continuity equation, we have,

$$\frac{\partial u}{\partial x} + \frac{\partial v}{\partial y} = 0. \tag{3.21}$$

The horizontal and vertical momentum equations in the lubrication approximations are given by,

$$\frac{\partial p}{\partial x} = \frac{\partial^2 u}{\partial y^2} - \alpha^2 u, \tag{3.22}$$

$$\frac{\partial p}{\partial y} = -\tilde{B}. \tag{3.23}$$

Also from equations (3.19) and (3.20) we have, at leading order in ϵ

$$p = -\frac{1}{\tilde{C}} \frac{\partial^2 h}{\partial x^2}, \quad \text{at} \quad y = h(x,t), \tag{3.24}$$

and

$$\frac{\partial u}{\partial y} = 0, \quad \text{at} \quad y = h(x,t). \tag{3.25}$$

Now integrating equation (3.23) with respect to y and use (3.24) to determine the integration constant. Since we don't want to keep the surface tension term, because we do not want to add complexity without significantly improving accuracy unless interfaces or sharp gradients are critical. then (3.24) will be equal to zero, thus we obtain,

$$p = -\tilde{B}(y - h). \tag{3.26}$$

Differentiating (3.26) with respect to x we have,

$$\frac{\partial p}{\partial x} = \tilde{B} \frac{\partial h}{\partial x} \tag{3.27}$$

The equation (3.27) is independent of y and hence (3.22) can be integrated directly to give a general equation as

$$u = Me^{\alpha y} + Ne^{-\alpha y} - \frac{1}{\alpha^2}\frac{\partial p}{\partial x}, \tag{3.28}$$

where $M = M(x,t)$ and $N = N(x,t)$. The no-slip boundary condition $u = 0$ at $y = 0$, and the tangential stress equation (3.25) are used to determine M and N, and the horizontal velocity is given by

$$u_{DB} = \frac{1}{\alpha^2}\frac{\partial p}{\partial x}\left[\frac{\cosh\alpha(h-y)}{\cosh(\alpha h)} - 1\right]. \tag{3.29}$$

Using equation (3.29) in (3.21), solving for v using no-penetration boundary condition and then applying to obtained v in equation (3.7) is equivalent to,

$$\frac{\partial h}{\partial t} + \frac{\partial \mathscr{R}}{\partial x} = 0, \quad \text{at} \quad y = h(x,t), \tag{3.30}$$

where,

$$\mathscr{R} = \int_0^h u dy, \tag{3.31}$$

using (3.31) we have that,

$$\mathscr{R} = -\frac{1}{\alpha^2}\frac{\partial p}{\partial x}\left[\frac{1}{\alpha}\tanh(\alpha h) - h\right], \quad at \quad y = h(x,t). \tag{3.32}$$

Substituting (3.32) and (3.27) into (3.30) we obtain a thin film equation

$$\frac{\partial h_{DB}}{\partial t} = \tilde{B}\frac{\partial}{\partial x}\left[\frac{1}{\alpha^2}\left(\frac{1}{\alpha}\tanh(\alpha h) - h\right)\frac{\partial h}{\partial x}\right]. \tag{3.33}$$

3.2 Asymptotic approximation in the limit $\alpha \to 0$ and $\alpha \to \infty$

Consider in (3.22), if $\alpha = 0$, then we find the solution,

$$u_{NS} = \frac{\partial p}{\partial x}\left[\frac{y^2}{2} - hy\right], \quad 0 < t \leq T, \quad x \in (0, L), \tag{3.34}$$

where the pressure gradient $\dfrac{\partial p}{\partial x}$ remains the same in the case of NS.
Using (3.31), $\mathscr{R}$ can be given as

$$\mathscr{R} = -\frac{1}{3}h^3\frac{\partial p}{\partial x}, \quad \text{at} \quad y = h(x,t), \tag{3.35}$$

and hence the thin film equation for h as given in (3.30) is

$$\frac{\partial h}{\partial t} = \frac{\partial}{\partial x}\left(\frac{1}{3}h^3\frac{\partial p}{\partial x}\right). \tag{3.36}$$

where, $\dfrac{\partial p}{\partial x}$ is found in (3.27) and this implies that

$$\frac{\partial h_{NS}}{\partial t} = \tilde{B}\frac{\partial}{\partial x}\left(\frac{1}{3}h^3\frac{\partial h}{\partial x}\right). \tag{3.37}$$

Note that we can't set $\alpha = 0$ directly from (3.29), but we can instead introduce an expansion in powers of the small parameter α as follows;

$$u_{DB} = u_0 + \alpha u_1 + \alpha^2 u_2 + ... \tag{3.38}$$

Expanding (3.29) in the limit of small α gives

$$u_0 = u_{NS} = \frac{\partial p}{\partial x}\left[\frac{1}{2}y^2 - hy\right], \quad u_1 = 0, \quad \text{and} \quad u_2 = \frac{\partial p}{\partial x}\left[\frac{1}{24}y^4 - \frac{1}{6}hy^3 + \frac{1}{3}h^3 y\right]. \tag{3.39}$$

The integral of the horizontal velocity expansion in (3.38), according to (3.31), becomes

$$\mathscr{R} = -\left[\frac{1}{3}h^3 - \frac{2}{15}h^5\alpha^2 + \frac{17}{315}h^7\alpha^4 - ...\right]\frac{\partial p}{\partial x} \tag{3.40}$$

substituting (3.40) into (3.30) we obtain,

$$\frac{\partial h_{DB}}{\partial t} = \frac{\partial}{\partial x}\left(\frac{h^3}{3}\frac{\partial p}{\partial x}\right) - \frac{\partial}{\partial x}\left(\frac{2h^5}{15}\alpha^2\frac{\partial p}{\partial x}\right) + \frac{\partial}{\partial x}\left(\frac{17h^7}{315}\alpha^4\frac{\partial p}{\partial x}\right) + ... \tag{3.41}$$

Setting $\alpha \to\ 0$ in (3.41) reduces to the corresponding evolution equation obtained from (NS), given in (3.36).

Also, in (3.22), if $\alpha \to\ \infty$, then the first term of its right-hand side which accounts for the viscous shear becomes negligible and we find the solution,

$$u_D = -\frac{1}{\alpha^2}\frac{\partial p}{\partial x}, \tag{3.42}$$

using (3.31), $\mathscr{R}$ can be given as

$$\mathscr{R} = -\frac{1}{\alpha^2}h\frac{\partial p}{\partial x}, \quad \text{at} \quad y = h(x,t), \tag{3.43}$$

now the thin film equation for h as given in (3.30) is

$$\frac{\partial h_D}{\partial t} = \tilde{B}\frac{\partial}{\partial x}\left(\frac{1}{\alpha^2}h\frac{\partial h}{\partial x}\right), \tag{3.44}$$

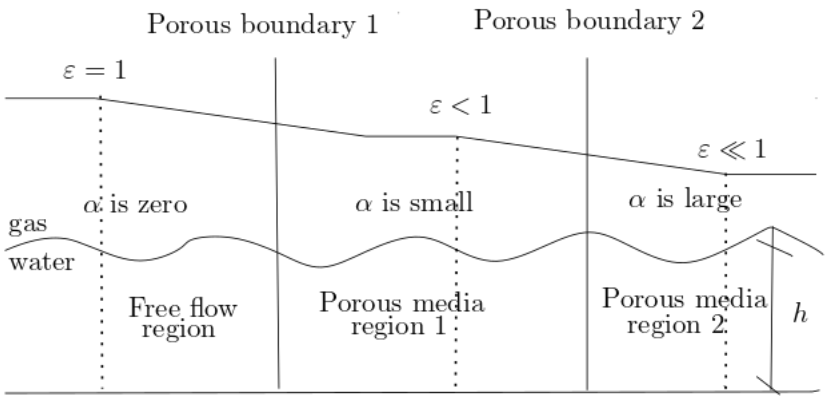

Figure 3.2: Transition through the boundary between free flow and porous media regions, where ε is a porosity of the material, as in [137].

Alternatively, taking the limit of (3.33) as α tends to zero is equal to (3.37). i.e.

$$\lim_{\alpha\to 0} \tilde{B}\frac{\partial}{\partial x}\left[\frac{1}{\alpha^2}\left(\frac{1}{\alpha}\tanh(\alpha h) - h\right)\frac{\partial h}{\partial x}\right] = \tilde{B}\frac{\partial}{\partial x}\left(\frac{1}{3}h^3\frac{\partial h}{\partial x}\right)$$

Also from (3.32), if the value of α is very large ($\alpha \to \infty$), then we have

$$\mathscr{R} = -\frac{1}{\alpha^2}h\frac{\partial p}{\partial x}, \quad \frac{1}{\alpha^3} \quad \text{is negligible.} \tag{3.45}$$

The thin film equation (3.33) is now equal to (3.44).

Alternatively, we can take the limit of (3.33) as α tends to ∞ for $\dfrac{1}{\alpha^3}$ to be negligible and this is equal to (3.44). i.e.

$$\lim_{\alpha\to \infty} \tilde{B}\frac{\partial}{\partial x}\left[\frac{1}{\alpha^2}\left(\frac{1}{\alpha}\tanh(\alpha h) - h\right)\frac{\partial h}{\partial x}\right] = \tilde{B}\frac{\partial}{\partial x}\left(\frac{1}{\alpha^2}h\frac{\partial h}{\partial x}\right)$$

Therefore the flow through a porous medium with infinitely large permeability ($k \to \infty$ is equivalent to $\alpha \to 0$) is the same as a simple flow of water, as expected. In the same manner the flow through a porous medium with very small permeability ($k \to 0$ is equivalent

to $\alpha \to \infty$) is the same as a simple flow of water in Darcy's experiment and can be simply shown in the equation and Figure (3.2),

$$\frac{\partial h_{DB}}{\partial t} = \begin{cases} \frac{\partial h_{NS}}{\partial t} & \text{if } \alpha \to 0 \\ \frac{\partial h_D}{\partial t} & \text{if } \alpha \to \infty \end{cases} \tag{3.46}$$

3.3 Steady state solution of DB at $\alpha = 0$ or ∞

Consider the equation (3.33) in the limit of $\alpha \to 0$ or ∞

$$\frac{\partial h}{\partial t} = \tilde{B}\frac{\partial}{\partial x}\left[rh^s\frac{\partial h}{\partial x}\right], \tag{3.47}$$

where r is an arbitrary constant and $s = 1$ or 3. At a steady state we have,

$$\frac{\partial h}{\partial t} = 0,$$

this implies that,

$$\frac{\partial}{\partial x}\left[h^s\frac{\partial h}{\partial x}\right] = 0. \tag{3.48}$$

Integrating (3.48) twice with respect to x, we obtain a general solution

$$h(x,t) = \left[(s+1)(Kx+D)\right]^{\frac{1}{s+1}}, \tag{3.49}$$

where K and D are arbitrary constants.

Using the boundary conditions, $h(0) = M$ and $h(L) = N$, we have,

$$D = \frac{M^{s+1}}{s+1}, \quad \text{and} \quad K = \frac{N^{s+1} - M^{s+1}}{(s+1)L}, \tag{3.50}$$

For example, if $L = 10$, $M = 0$, and $N = 1$, we obtain a steady state solution to be

$$h(x,t) = (0.1x)^{\frac{1}{s+1}}. \tag{3.51}$$

3.4 Numerical methods

In our study, we employed Chebfun as a powerful computational tool to investigate the complex flow dynamics arising from the coupling of Navier-Stokes equations for free surface flow and Brinkman equations for flow through porous media. Chebfun's ability to handle high-order polynomial approximations and efficiently compute solutions to differential equations made it an ideal choice for our numerical simulations [24], [119], [143]. By utilizing Chebfun to solve the thin film equations in the porous media, we were able to accurately capture the intricate flow behavior within the porous structure, accounting for both viscous and inertial effects. The numerical results provided detailed insight into fluid flow patterns occurring in the porous medium under the influence of the Brinkman model. Furthermore, by integrating the solutions obtained from Chebfun with the thin film equations modeling the free surface flow, we observed the dynamic interaction between the free surface and porous media flows. The numerical simulations allowed us to analyze how the presence of the porous medium affects the behavior of the free surface, leading to a comprehensive understanding of the coupled flow system. Using Chebfun, we were able to efficiently analyze and visualize the numerical results, facilitating the interpretation of the complex flow phenomena emerging from the Navier-Stokes and Brinkman equations. The integration of Chebfun into our computational framework enhanced the accuracy and reliability of our simulations, highlighting the utility of Chebfun in studying multiphase flow problems.

3.4.1 Numerical results

The lubrication equation (3.33) is solved numerically using a Chebfun method on a domain of $[0,\ L]$ and a variable time step size is found to be sufficient to produce accurate results with sinusoidal, Gaussian, and wave packet initial conditions of the form,

$$h(x,0) = h_0\left[1 + h_A \sin\left(\frac{m\pi x}{L}\right)\right] \tag{3.52}$$

$$h(x,0) = h_0\left[1 + h_A \exp\left(\frac{x - x_0}{b}\right)^2\right] \tag{3.53}$$

$$h(x,0) = h_0\left[1 + h_A \exp\left(\frac{x - x_0}{b}\right)^2 \sin\left(\frac{m\pi x}{L}\right)\right] \tag{3.54}$$

where, $b = 0.14$, $h_0 = 0.1$, $h_A = 0.5$, $L = 10$ and m is a frequency. Dirichlet boundary conditions are imposed on both ends of the computational domain, $x = 0$ and $x = L$. The solutions of (3.33), (3.37), and (3.44) are given in the figures below.

From the numerical calculation, it can be observed that the permeability of the porous medium decreases when we increase α. In Figure 3.3a, 3.4a and 3.5a, we present the plot of the surfaces h, of thin film flow for the solutions of (3.36) and (3.41) using the same or different initial conditions (3.52), (3.53), and (3.54) for the value of $\alpha = 0$. It is observed that the figures of the two solutions of the same initial condition show similar surface h. In Figures 3.3b, 3.4b, and 3.5b, we plot the surfaces h, of thin film flow, for the solution of (3.33) using different initial conditions (3.52), (3.53), and (3.53) for the value of $\alpha = 1$. It was observed that the deformation of the surface shows the effect of the non-linearity of the equation. In Figures 3.3c, 3.4c, and 3.5c, we plot the surfaces h, of thin film flow, for the solution of (3.33) using two different initial conditions (3.52), (3.53), and (3.53) for the value of $\alpha = 2$. Each curve presents a surface different from the above figure due to the increase in time and value of α. Similarly, it continues up to Figures 3.3f, 3.4f, and 3.5f where we plot

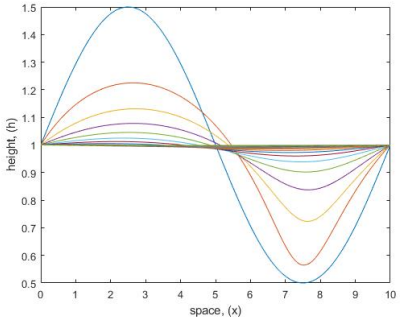

(a) Plot of surface h for α =0

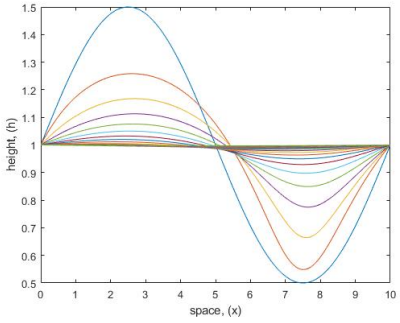

(b) Plot of surface h for α =1

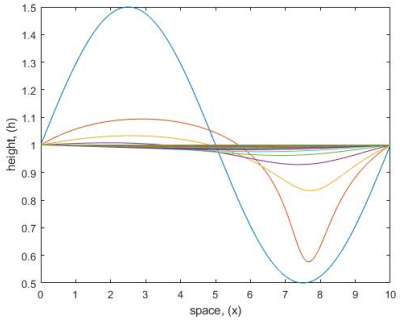

(c) Plot of surface h for α =2

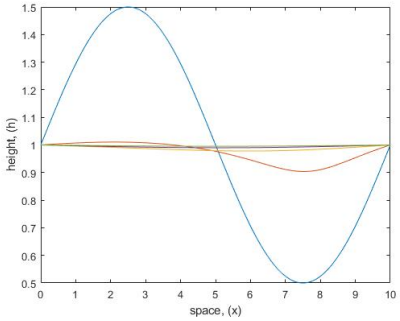

(d) Plot of surface h for α =3

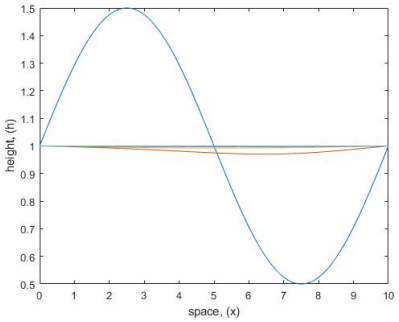

(e) Plot of surface h for α =4

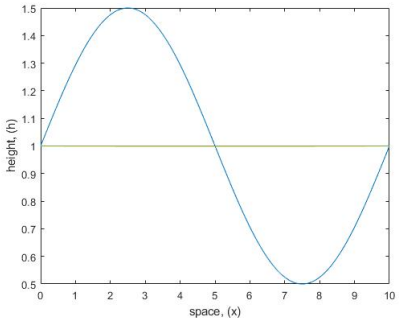

(f) Plot of surface h for α =5

Figure 3.3: Plot of the surface profile h at different times, obtained from a time-dependent calculation of equations (3.33) *and* (3.37) *with Dirichlet boundary condition, starting from an initial condition of the equation* (3.52)*, with $h_0 = 0.1$, $h_A = 0.5$, $m = 2$, and $L = 10$. For each panel, present the solution corresponding to each value of α as indicated in the sub-caption.*

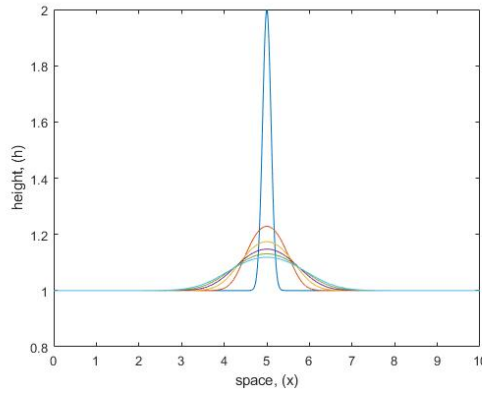

(a) Plot of surface h for α =0

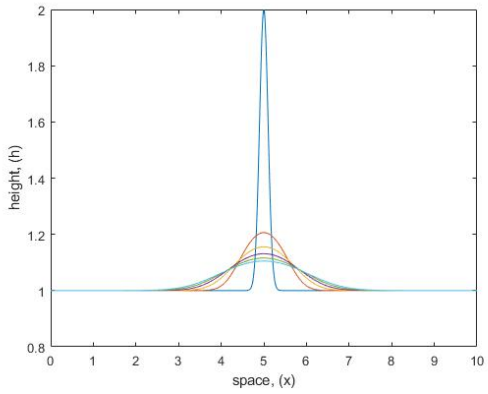

(b) Plot of surface h for α =1

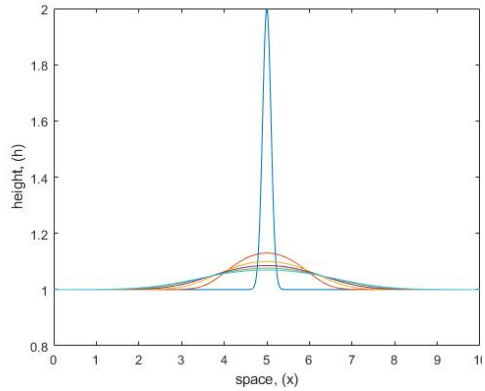

(c) Plot of surface h for α =2

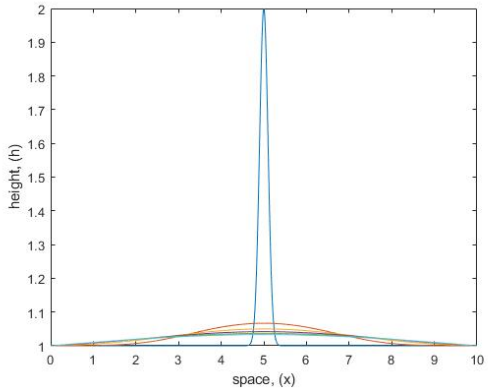

(d) Plot of surface h for α =3

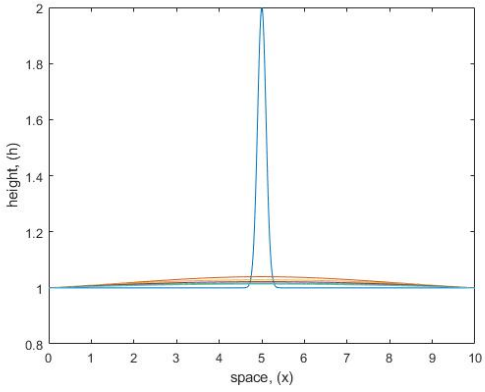

(e) Plot of surface h for α =4

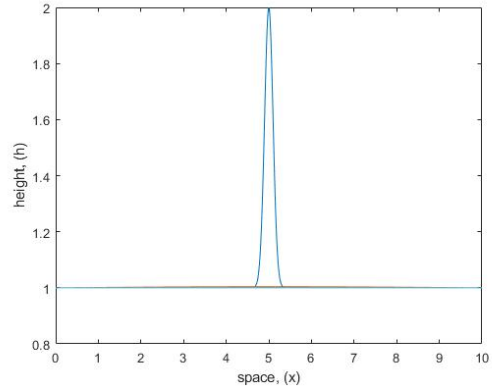

(f) Plot of surface h for α =5

Figure 3.4: Plot of the surface profile h at different times, obtained from a time-dependent calculation of equations (3.33) *and* (3.37) *with Dirichlet boundary condition, starting from an initial condition of the equation* (3.53)*, with* $h_0 = 0.1$*,* $h_A = 0.5$*,* $m = 2$*, and* $L = 10$*. For each panel, present the solution corresponding to each value of* α *as indicated in the sub-caption.*

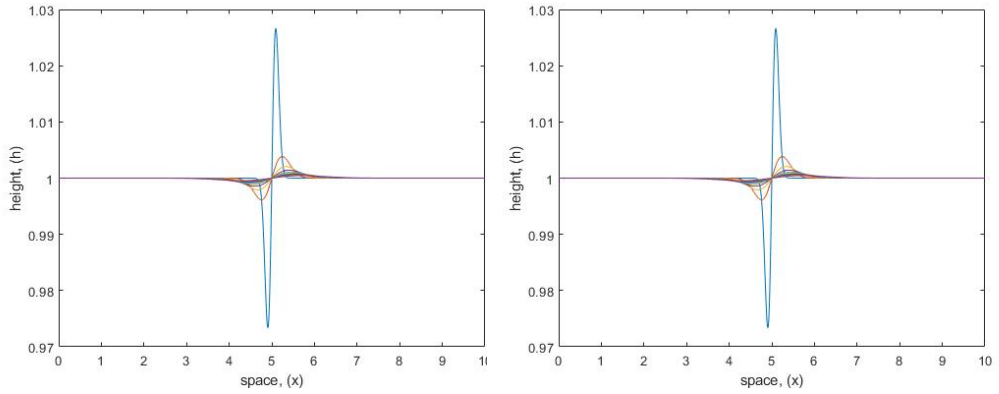

(a) Plot of surface h for α =0

(b) Plot of surface h for α =1

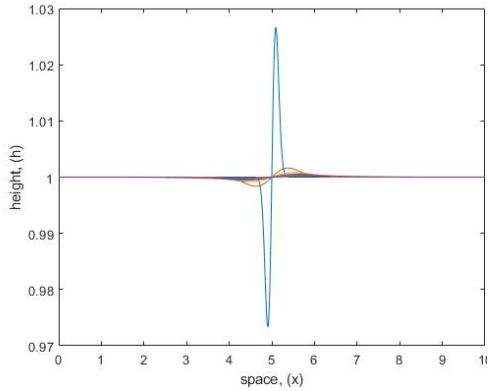

(c) Plot of surface h for α =2

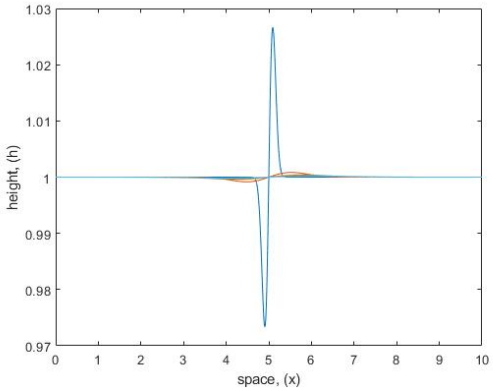

(d) Plot of surface h for α =3

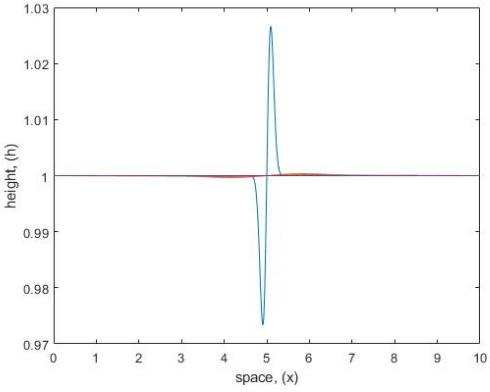

(e) Plot of surface h for α =4

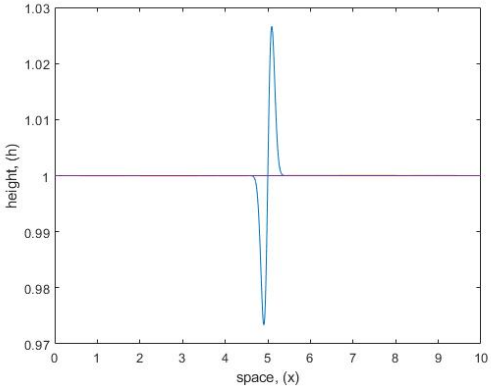

(f) Plot of surface h for α =5

Figure 3.5: Plot of the surface profile h at different times, obtained from a time-dependent calculation of equations (3.33) *and* (3.37) *with Dirichlet boundary condition, starting from an initial condition of the equation* (3.54)*, with* $h_0 = 0.1$*,* $h_A = 0.5$*,* $m = 2$*, and* $L = 10$*. For each panel, present the solution corresponding to each value of* α *as indicated in the sub-caption.*

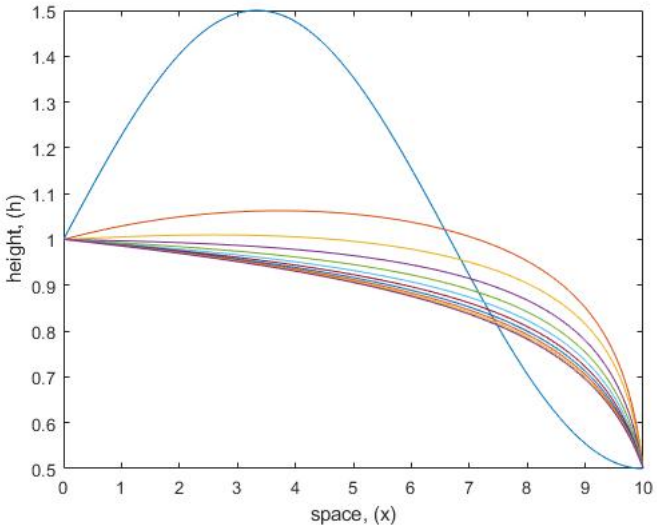

Figure 3.6: Free surface profile h at different times, obtained from a time-dependent calculation of equations (3.33) *with Dirichlet boundary condition, starting from an initial condition of the equation* (3.52)*, with* $h_A = 0.5, m = 1.5,$ *and* $L = 10.$*, the other parameter is* $\alpha = 2$

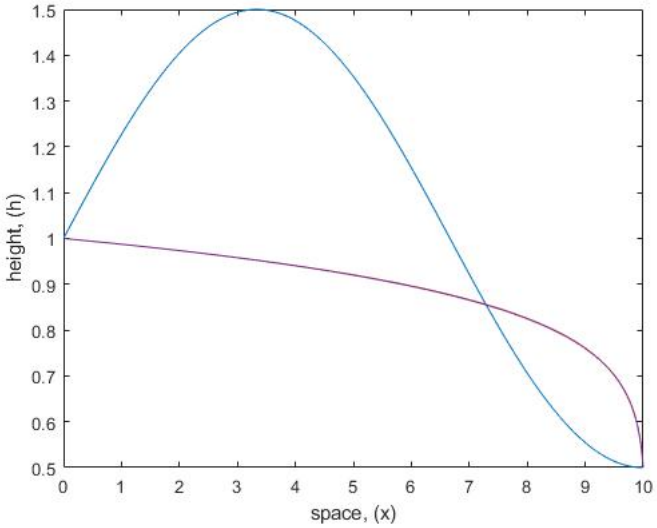

Figure 3.7: Free surface profile h at different times, obtained from a time-dependent calculation of equations (3.33) *with Dirichlet boundary condition, starting from an initial condition of the equation* (3.52)*, with* $h_A = 0.5, m = 1.5,$ *and* $L = 10.$*, the other parameter is* $\alpha = 4$

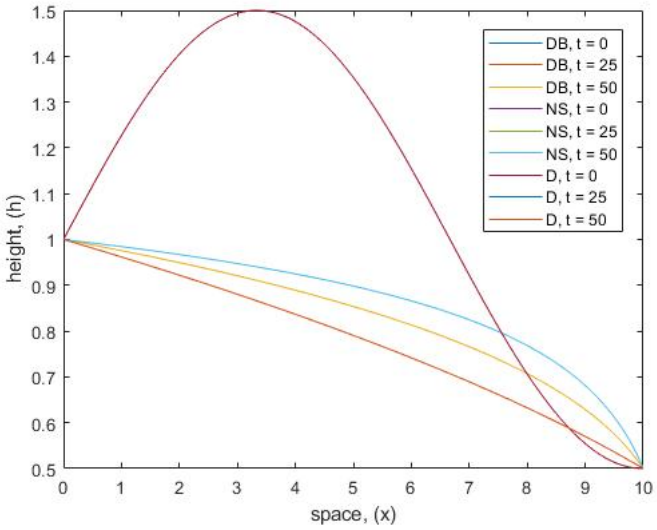

Figure 3.8: Free surface profile h at different times, obtained from a time-dependent calculation of equations (3.33),(3.37) *and* (3.44) *with Dirichlet boundary condition, starting from an initial condition of the equation* (3.52)*, with* $h_A = 0.5, m = 1.5$*, and* $L = 10.$*, the other parameter is* $\alpha = 4$

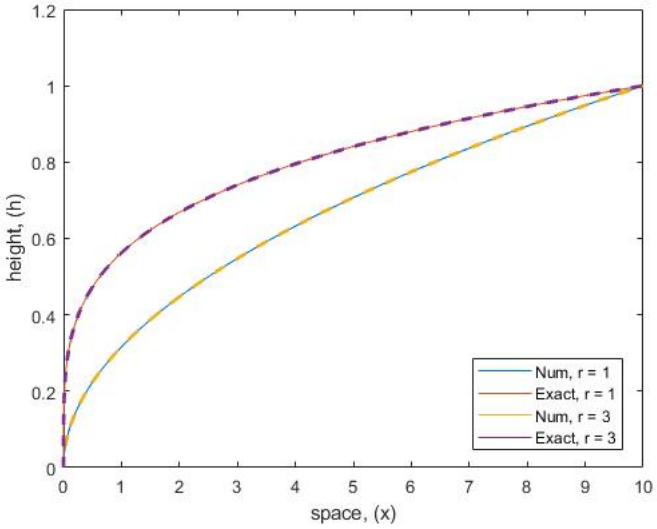

Figure 3.9: Plot of surface profile h, obtained from a steady state solution (3.51) *and the numerical solution of equation* (3.47) *with* $r = 1$ *and* 3

the surfaces h, of thin film flow, for the solution of (3.33) using different initial conditions (3.52), (3.53), and (3.54) for the value of $\alpha = 5$. Each curve presents a surface at a different time and turns flat at the time-end. It is generally observed from the comparison that a higher value of α produces waves with reducing amplitude and move faster and attain a steady state at $\alpha = 5$. Figure 3.6 and 3.7, show interesting results of the two surface profile h, for the solution of equations (3.33) using initial condition (3.52) at different times. Here we used Dirichlet boundary conditions different from the ones used in Figures 3.3a, 3.3b, etc. It was observed that the surface curves do not turn flat at the time-end. In Figure 3.8, we plot the surfaces h for the solution of (3.33), (3.37), and (3.44) at different times using initial condition (3.52) and Dirichlet boundary condition used in Figures 3.6 and 3.7. It is observed that the surface with D turned flat faster than the one with NS and DB always lies between them.

Note that α is constant if the permeability k is constant or homogeneous and the above cases are considered when α is constant. In Figures 3.9 , we plot the surface h for the steady solutions of the equation (3.47).

3.5 Heterogeneous permeability

Naturally occurring porous media display some level of spatial permeability variation, called heterogeneous permeability. Few porous media have homogeneous permeability, although some have more variables than others. That is the permeability of smaller volumes of rocks will be different from the permeability of a large volume within it. Here we consider non-constant or heterogeneous permeability with spatial variation, i.e. $k = k(y)$ or $k(x)$.

Now, if we let $\alpha = \alpha(y)$, the thin film equation (3.44) becomes,

$$\frac{\partial h_D}{\partial t} = \tilde{B}\frac{\partial}{\partial x}\left[\int_0^h k(y)dy\frac{\partial h}{\partial x}\right], \quad k(y) = \frac{1}{\alpha^2(y)}. \tag{3.55}$$

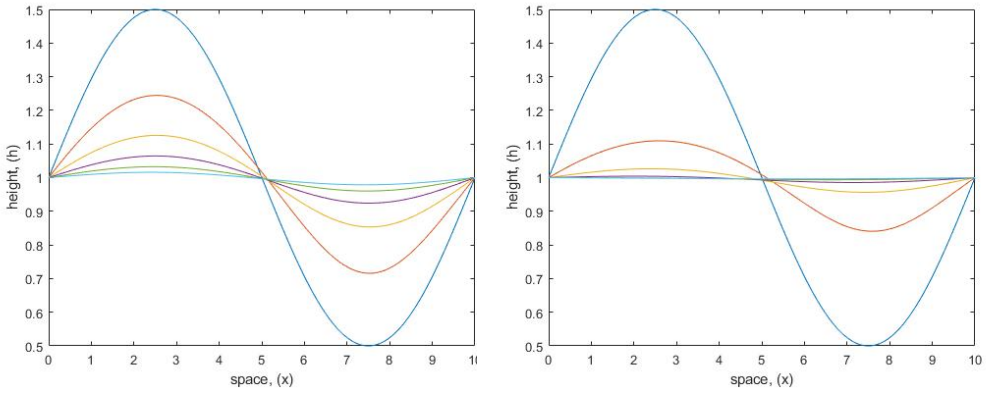

(a) Plot of surface h, with $k(y) = a\cos(y)$ *(b) Plot of surface h, with $k(y) = ae^{y}$*

Figure 3.10: Free surface profile h at different times, obtained from a time-dependent calculation of equations (3.55) *and Dirichlet boundary condition, starting from an initial condition of the equation* (3.52)*, with $h_A = 0.5, m = 2$, and $L = 10.$, the other parameter is $a = 1$*

Similarly, for $\alpha = \alpha(x)$, we can have,

$$\frac{\partial h_D}{\partial t} = \tilde{B}\left[\frac{\partial}{\partial x}\left(k(x)\frac{\partial h}{\partial x}\right)h + k(x)\left(\frac{\partial h}{\partial x}\right)^2\right], \quad k(x) = \frac{1}{\alpha^2(x)}. \tag{3.56}$$

From the thin film equation (3.55), if we let $k(y) = a\cos(y)$ or $k(y) = ae^{y}$, and $k(x) = ae^{x}$ or $k(x) = ae^{-x}$ from (3.56), then solutions are given in the Figures 3.10, 3.11, 3.12 and 3.13.

In Figures 3.10a, 3.10b, 3.11a, and 3.11b, we plot the surfaces h, of thin film flow, for the solution of (3.55) using initial conditions (3.52) and (3.53) for heterogeneous permeabilities, $k(y) = a\cos(y)$ and $k(y) = ae^{y}$ respectively. It was observed that the deformation of the surfaces shows the same effect as the one with homogeneous permeability, this is due to the thin nature of fluids. Similarly, in Figure 3.12a and 3.13a, the surface h is plotted for the solution of (3.56) using initial (3.52) for $k(x) = ae^{x}$, and this shows that the deformation is in positive x-direction. Finally, in Figure 3.10b and 3.11a, we plot the surface h of thin flow, for the solution of (3.56) using initial (3.52) and (3.53) for heterogeneous permeability $k(x) = ae^{-x}$.

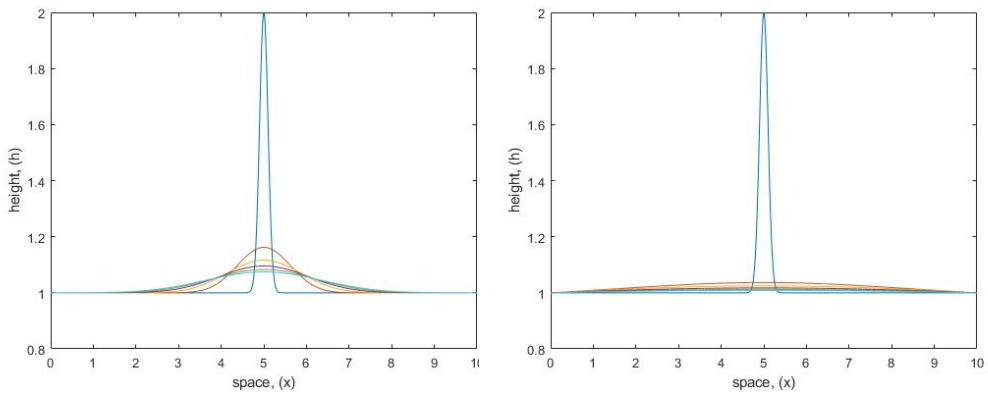

(a) Plot of surface h, with $k(y) = a\cos(y)$ *(b) Plot of surface h, with $k(y) = ae^{y}$*

Figure 3.11: Free surface profile h at different times, obtained from a time-dependent calculation of equations (3.55) *and Dirichlet boundary condition, starting from an initial condition of the equation* (3.53)*, with $h_A = 0.5, m = 2$, and $L = 10.$, the other parameter is $a = 1$*

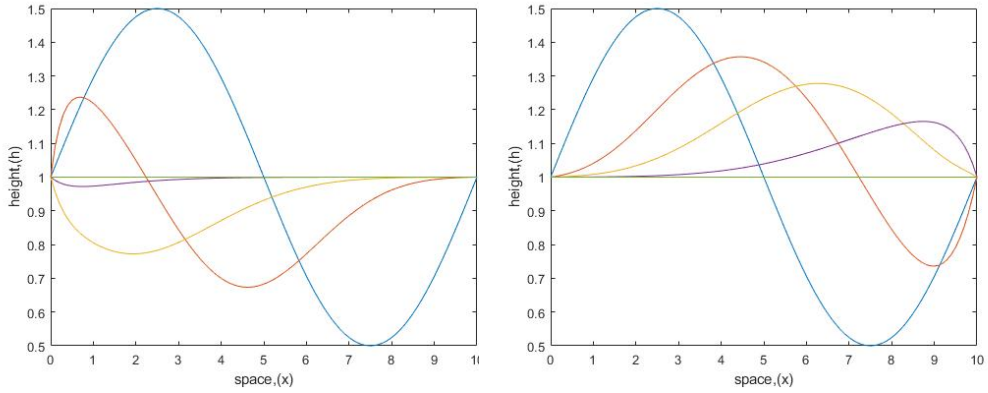

(a) Plot of surface h, with $k(x) = ae^{x}$ *(b) Plot of surface h, with $k(x) = ae^{-x}$*

Figure 3.12: Free surface profile h at different times, obtained from a time-dependent calculation of equations (3.56) *and Dirichlet boundary condition, starting from an initial condition of the equation* (3.52)*, with $h_A = 0.5, m = 2$, and $L = 10.$, the other parameter is $a = 1$*

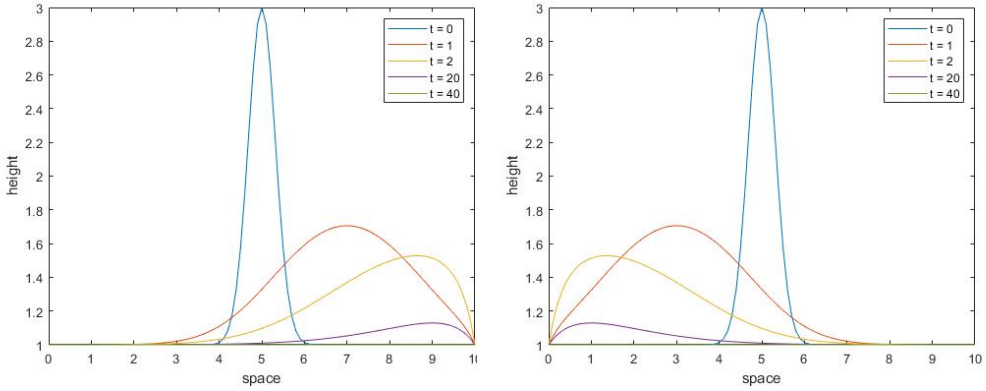

(a) Plot of surface h, with $k(x) = ae^{x}$ *(b) Plot of surface h, with $k(x) = ae^{-x}$*

Figure 3.13: Free surface profile h at different times, obtained from a time-dependent calculation of equations (3.56) *and Dirichlet boundary condition, starting from an initial condition of the equation* (3.53)*, with $h_A = 0.5, m = 2$, and $L = 10.$, the other parameter is $a = 1$*

Chapter 4

Two fluids with an interface

Consider two stratified immiscible fluids (fluid 1 and fluid 2) in a porous medium bounded below and above by horizontal walls and separated by a sharp interface between them as given in Figure 4.1 below. We define ρ_1, ρ_2, and μ_1, μ_2 as the densities and viscosities of the fluids and denote subscripts 1 and 2 for the bottom and top fluids, respectively. We also defined x and y as horizontal and vertical Cartesian coordinates and t as time in seconds. The lower fluids extend from $y = 0$ to the interface at $y = h(x, t)$, while the upper fluids extend from the interface at $y = h(x, t)$ to $y = H$ for $H = 1$.

4.1 Thin film of two fluids in porous media

In porous media, such as a material with small empty spaces or pores, the presence of two fluids forming a thin film can have interesting implications. The formation of a thin film of two fluids in a porous medium can be influenced by factors such as the permeability of the porous material, the interfacial forces between the fluids, and the pore structure of the medium [44, 128]. These factors determine the stability, thickness, and dynamics of the thin film. In this, the thin film of two fluids in a porous medium will be compared with one of a

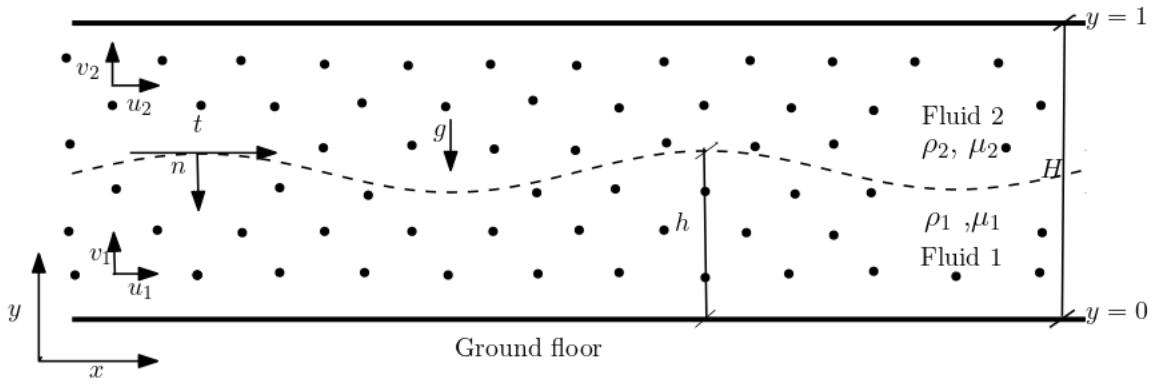

Figure 4.1: Sketch of two immiscible stratified fluids with a sharp separating interface. The horizontal and vertical velocities are given as u_i and v_i, for $i = 1, 2$ respectively.

surface when the value of α tends to zero or infinity as in the case above.

When α approaches zero, this physically represents a situation where the porous medium has very low permeability, making the effects of the porous structure almost insignificant. In this case, the thin film acts as if it's resting on a solid, impermeable surface, with the flow dynamics mainly influenced by surface tension, viscosity, and interfacial forces, without much fluid interaction with the substrate.

Conversely, when α approaches infinity, it signifies a highly permeable porous medium where the interaction between the fluid and the pore structure becomes dominant. Here, the thin film can be significantly influenced by capillary action and fluid drainage into the medium, resulting in different stability and thickness characteristics compared to a film on a non-porous surface.

4.1.1 Governing Equation

Like in a single fluid, the continuity and momentum equations in two fluids are given as;

$$\nabla \cdot \mathbf{u}_i = 0, \quad \mu_i \nabla^2 \mathbf{u}_i = \nabla p_i + \rho_i \mathbf{g}, \quad \text{(Stokes equation)} \tag{4.1}$$

$$\nabla \cdot \mathbf{u}_i = 0, \quad \mathbf{u}_i = -\frac{k}{\mu} \nabla p_i + \rho_i \mathbf{g}, \quad \text{(Darcy equation)} \tag{4.2}$$

$$\nabla \cdot \mathbf{u}_i = 0, \quad \mu_i \nabla^2 \mathbf{u}_i - \frac{\mu_i}{k} \mathbf{u}_i = \nabla p_i + \rho_i \mathbf{g}, \quad \text{(Brinkman equation)} \tag{4.3}$$

where $\mathbf{u}_i$, μ_i, p_i, and ρ_i are the velocities, viscosities, pressures, and densities in each fluid layer, denoted by a subscript $i = 1, 2$. Note that the Stokes equation (4.1) is a simplified version of the N-S, derived under the assumption that inertial forces are negligible compared to viscous forces and this occurs when the low Reynolds numbers of the flow are very small i.e $Re \ll 1$.

4.1.2 Conditions on the boundaries

The imposed boundary conditions at the bottom and upper walls are;

no-slip:

$$u_1 = 0 \quad \text{at} \quad y = 0, \quad u_2 = 0 \quad \text{at} \quad y = 1, \tag{4.4}$$

and no-penetration:

$$v_1 = 0 \quad \text{at} \quad y = 0, \quad v_2 = 0 \quad \text{at} \quad y = 1. \tag{4.5}$$

4.1.3 Conditions at the interface between the fluids

At the interface, both horizontal and vertical velocities are continuous, i.e.

$$u_1 = u_2 \quad \text{and} \quad v_1 = v_2 \tag{4.6}$$

and the kinematic equation becomes,

$$v_1 = \frac{\partial h}{\partial t} + u_1 \frac{\partial h}{\partial x} \tag{4.7}$$

According to [74] the stress jump at the interface is given by

$$\mathbf{n} \cdot (\boldsymbol{\sigma_1} - \boldsymbol{\sigma_2}) = \kappa\gamma, \tag{4.8}$$

where γ is surface tension coefficient, $\boldsymbol{\sigma_1}$ and $\boldsymbol{\sigma_2}$ are stress tensors in fluids 1 and 2 respectively, and are generally defined as

$$\boldsymbol{\sigma_i} = -p_i \mathbb{I} + \mu_i(\nabla \mathbf{u}_i + (\nabla \mathbf{u}_i)^T), \quad i = 1, 2 \tag{4.9}$$

where $\mathbb{I}$ is an identity matrix. The unit normal $\mathbf{n}$, the unit tangent $\mathbf{t}$, and the curvature κ of the interface are given respectively as in the equation (3.10). The normal stress condition is obtained by taking the dot product of equation (4.8) with a unit normal $\mathbf{n}$, while the tangential stress condition is also obtained by taking the dot product of (4.8) with the unit tangent $\mathbf{t}$ to give,

$$[\mathbf{n} \cdot (\mathbf{n} \cdot \boldsymbol{\sigma})]_2^1 = \kappa\gamma, \quad [\mathbf{t} \cdot (\mathbf{n} \cdot \boldsymbol{\sigma})]_2^1 = 0, \tag{4.10}$$

where $[e_i]_2^1 = e_1 - e_2$.

The normal and tangential stress in a subscript notation are given by

$$\left[\frac{2\mu_i}{1 + h_x^2} \left[u_{ix} h_x^2 + v_{iy} - (v_{iy} + u_{ix}) h_x \right] - p + p h_x^2 \right]_2^1 = \frac{\gamma h_{xx}}{(1 + h_x^2)^{3/2}} \tag{4.11}$$

and

$$\left[4\mu_i u_{ix} h_x + \mu_i (1 - h_x^2)(u_{iy} - v_{ix}) \right]_2^1 = 0 \tag{4.12}$$

4.1.4 Non-dimensionalisation

We introduce non-dimensional variables by performing some transformations of the following,

$$x = l_0 x^*, \quad y = h_0 y^*, \quad u_i = U_0 u_i^*, \quad v_i = V_0 v_i^* \quad t = \frac{l_0}{U_0} t^* \quad p_i = \frac{\mu_1 U_0 l_0}{h_0^2} p_i^*, \tag{4.13}$$

Note that the parameters $m_1 = 1$, $m_2 = m$, $n_1 = 1$, $n_2 = n$, where $m_i = \dfrac{\rho_i}{\rho_1}$ and $n_i = \dfrac{\mu_i}{\mu_1}$ to be density and viscosity ratio respectively. The non-dimensional continuity and (DB) equation for the flow in each fluid region are given as,

$$\frac{U_0}{l_0}\frac{\partial u_i}{\partial x} + \frac{V_0}{h_0}\frac{\partial v_i}{\partial y} = 0, \tag{4.14}$$

here we impose the condition (3.15) and

$$u_i = \alpha^{-2}\left[\epsilon^2 \frac{\partial^2 u_i}{\partial x^2} + \frac{\partial^2 u_i}{\partial y^2} - \frac{1}{n_i}\frac{\partial p_i}{\partial x}\right] \tag{4.15}$$

$$\epsilon^2 v_i = \alpha^{-2}\left[\epsilon^2\left(\epsilon^2 \frac{\partial^2 v_i}{\partial x^2} + \frac{\partial^2 v_i}{\partial y^2}\right) - \frac{1}{n_i}\frac{\partial p_i}{\partial y} - \frac{m_i}{n_i}\tilde{B}\right], \tag{4.16}$$

where, $\epsilon = \dfrac{h_0}{l_0}$ is a height-to-length ratio, $\alpha = \dfrac{h_0}{\sqrt{k}}$ is a dimensionless parameter defined in terms of k, the permeability parameter, $\tilde{B} = \epsilon B$, and B is a number defined by $\dfrac{1}{\epsilon}\dfrac{\rho_1}{\mu_1}\dfrac{h_0^2}{U_0} g$.

Also, the non-dimensional normal and tangential stress jumps at the interface in sub-scripts notation are given by

$$\left[2\epsilon^2\left[\epsilon^2 h_x^2 u_{ix} + v_{iy} - (h_x u_{iy} + \epsilon h_x v_{ix})\right] - (p_i + \epsilon^2 h_x^2 p_i)\right]_2^1 = \frac{1}{\tilde{C}}\frac{h_{xx}}{(1+\epsilon^2 h_x^2)^{1/2}} \quad \text{at} \quad y = h(x,t), \tag{4.17}$$

$$\left[4\epsilon^2 h_x (u_{ix}) + (1 - \epsilon^2 h_x^2)(u_{iy} - \epsilon^2 v_{ix})\right]_2^1 = 0 \quad \text{at} \quad y = h(x,t), \tag{4.18}$$

where $\tilde{C} = \dfrac{C}{\epsilon^3}$ and C is a capillary number defined by $\dfrac{\mu_1 U_0}{\gamma}$.

Role of Buoyancy in Terms of Density Ratio m

The relative density difference can be expressed as

$$1 - m = \frac{\rho_i - \rho_1}{\rho_i} \tag{4.19}$$

This quantity $1 - m$ appears naturally in non-dimensionalized equations when accounting for buoyancy effects. The buoyancy force per unit volume is given by:

$$\Delta\rho \cdot g = (\rho_i - \rho_1)g = \rho_i g(1 - m) \tag{4.20}$$

Thus, the magnitude of buoyancy is directly proportional to $1-m$. The physical implications are as follows:

- If $m = 1$, then $1 - m = 0$: there is no buoyancy since the fluid densities are equal.
- If $m < 1$, then $1 - m > 0$: the upper fluid is lighter, leading to a buoyancy force that can drive instabilities (e.g., Rayleigh–Taylor instability).
- If $m > 1$, then $1 - m < 0$: the upper fluid is heavier, and buoyancy may act in a stabilizing manner.

In many thin film or porous media flow models, the gravity-induced term may appear in a non-dimensional form such as:

$$(1 - m) \cdot G$$

where, G represents a gravitational group (e.g., a Bond number).

4.1.5 Lubrication approximation

As in the subsection (3.1.5), the leading order continuity and momentum equations in each fluid $i = 1, 2$, are the lubrication equations, given by,

$$\frac{\partial u_i}{\partial x} + \frac{\partial v_i}{\partial y} = 0 \tag{4.21}$$

$$\frac{\partial^2 u_i}{\partial y^2} - \alpha^2 u_i = \frac{1}{n_i}\frac{\partial p_i}{\partial x} \tag{4.22}$$

$$\frac{\partial p_i}{\partial y} = -m_i \tilde{B}, \tag{4.23}$$

and the leading order normal and tangential stress balances at the interface are

$$-p_1 + p_2 = \frac{1}{\tilde{C}}\frac{\partial^2 h}{\partial x^2}, \quad \text{at} \quad y = h(x,t), \tag{4.24}$$

$$\frac{\partial u_1}{\partial y} - n\frac{\partial u_2}{\partial y} = 0, \quad \text{at} \quad y = h(x,t), \tag{4.25}$$

integrating (4.23) in y gives

$$p_i = -m_i \tilde{B} y + \tilde{p_i}, \tag{4.26}$$

where p_i are related to each other through equation (4.24), as in [75]

$$p_2 = p_1 + f, \quad f = \left[\tilde{B}h + \frac{1}{\tilde{C}}\frac{\partial^2 h}{\partial x^2}\right]. \tag{4.27}$$

The momentum equation (4.22) can be integrated in y to give a solution

$$u_i = M_i e^{\alpha y} + N_i e^{-\alpha y} - \frac{n_i^{-1}}{\alpha^2}\frac{\partial p_i}{\partial x} \tag{4.28}$$

where $M_i = M_i(x,t)$ and $N_i = N_i(x,t)$. The no-slip boundary conditions on $u_1 = 0$ at $y = 0$, and $u_2 = 0$ at $y = 1$, are used to determine N_i. The horizontal velocities are given by,

$$u_1 = M_1[e^{\alpha y} - e^{-\alpha y}] + \frac{1}{\alpha^2}\frac{\partial p_1}{\partial x}\left[e^{-\alpha y} - 1\right] \tag{4.29}$$

$$u_2 = M_2[e^{\alpha y} - e^{-\alpha(y-2)}] + \frac{n^{-1}}{\alpha^2}\frac{\partial p_2}{\partial x}\left[e^{-\alpha(y-1)} - 1\right] \tag{4.30}$$

and using no-penetration conditions on $v_1 = 0$ at $y = 0$, and $v_2 = 0$ at $y = 1$, with the continuity equation (4.21) to determine the vertical velocities which are given as

$$v_1 = -\frac{1}{\alpha}\frac{\partial M_1}{\partial x}\left[e^{\alpha y} + e^{-\alpha y} - 2\right] + \frac{1}{\alpha^3}\frac{\partial^2 p_1}{\partial x^2}\left[e^{-\alpha y} + \alpha y - 1\right] \tag{4.31}$$

$$v_2 = -\frac{1}{\alpha}\frac{\partial M_2}{\partial x}\left[e^{\alpha y} + e^{-\alpha(y-2)} - 2e^{\alpha}\right] + \frac{n_2^{-1}}{\alpha^3}\frac{\partial^2 p_2}{\partial x^2}\left[e^{-\alpha(y-1)} + \alpha y - \alpha - 1\right] \tag{4.32}$$

substituting (4.29) and (4.31) into (4.7) we can obtain,

$$\frac{\partial h}{\partial t} + \frac{\partial \mathscr{R}}{\partial x} = 0, \quad \text{at} \quad y = h(x,t). \tag{4.33}$$

We now define,

$$\mathscr{R} = \int_0^h u_1 dy, \tag{4.34}$$

M_i can be determined by using first equation of (4.6) and (4.25) then using first term of (4.27). Their expressions are simplified to

$$M_2 = \frac{1}{n}\left[M_1 + \frac{1}{\alpha^2 e^{2\alpha y+1}}\frac{\partial f}{\partial x}\right] \tag{4.35}$$

$$M_1 = \frac{[(n-1)e^{2\alpha y} + n - 1]\dfrac{\partial p}{\partial x} + (e^{\alpha y} - 1)\dfrac{\partial f}{\partial x}}{[(n-1)(e^{3\alpha y} + e^{2\alpha y} + e^{\alpha y}) - 4e^{\alpha y} + n]\alpha^2} \tag{4.36}$$

According to [24], [75], and [111],satisfying (4.6) is equivalent to solving the flow rate $Q(t)$, defined as

$$Q(t) = \int_0^h u_1 dy + \int_h^1 u_2 dy, \tag{4.37}$$

and this leads to determining the leading order pressure gradient given by

$$\frac{\partial p_1}{\partial x} = \Gamma(\alpha, n). \tag{4.38}$$

Also, substituting,(4.36) and (4.38) into (4.29) and then (4.34) we obtain,

$$\mathscr{R} = S(\alpha, n) \quad \text{at} \quad y = h(x, t). \tag{4.39}$$

The functions $\Gamma(\alpha, n)$ and $S(\alpha, n)$ depend on α and n. Their exact expressions, which are too lengthy to present here, have been obtained using the numerical software *Maple* and will be provided in Appendix A. Putting (4.39) into (4.33), we obtain the thin film equation to be

$$\frac{\partial h}{\partial t} = -\frac{\partial S(\alpha, n)}{\partial x} \tag{4.40}$$

4.2 Thin film of two fluids in a non-porous mediun

This section is closely the same as [76], with a minor difference in the boundary conditions and is also presented here for completeness. Considering the continuity and momentum equations (4.1), boundary conditions (4.4),(4.5) and conditions at the interface (4.6),(4.7). The non-dimensional continuity and Navier Stokes equation for the flow in each fluid region

for fluids $i = 1, 2$ are given by (4.14), and

$$\epsilon^2 \frac{\partial^2 u_i}{\partial x^2} + \frac{\partial^2 u_i}{\partial y^2} = \frac{1}{n_i} \frac{\partial p_i}{\partial x}, \tag{4.41}$$

$$\epsilon^2 \left[\epsilon^2 \frac{\partial^2 v_i}{\partial x^2} + \frac{\partial^2 v_i}{\partial y^2} \right] = \frac{1}{n_i} \frac{\partial p_i}{\partial y} + \frac{m_i}{n_i} \epsilon \tilde{B}. \tag{4.42}$$

The non-dimensional normal and tangential stress jumps at the interface are given by (4.17) and (4.18). The leading order continuity and momentum equations in each fluid $i = 1, 2$, are the lubrication equations, given by (4.21), (4.23) and

$$\frac{\partial p_i}{\partial x} = n_i \frac{\partial^2 u_i}{\partial y^2}, \tag{4.43}$$

Also, the leading order normal and tangential stress balances at the interface are given by (4.24) and (4.25). The momentum equation (4.43) can be integrated twice in y to give a general equation

$$u_i = \frac{1}{2n_i} \frac{\partial p_i}{\partial x} y^2 + M_i y + N_i, \quad i = 1, 2. \tag{4.44}$$

where $M_i = M_i(x, t)$ and $N_i = N_i(x, t)$. The no-slip boundary conditions on $u_1 = 0$, at $y = 0$ and $u_2 = 0$, at $y = 1$ are used to determine N_i, the horizontal velocities are given by,

$$u_1 = \frac{1}{2} \frac{\partial p_1}{\partial x} y^2 + M_1 y, \tag{4.45}$$

$$u_2 = \frac{1}{2n} \frac{\partial p_2}{\partial x} (y^2 - 1) + M_2 (y - 1), \tag{4.46}$$

and using no-penetration conditions on $v_1 = 0$ at $y = 0$ and $v_2 = 0$ at $y = 1$, and (4.21) to determine the vertical velocities which are given as

$$v_1 = -\frac{1}{6} \frac{\partial^2 p_1}{\partial x^2} y^3 - \frac{1}{2} \frac{\partial M_1}{\partial x} y^2, \tag{4.47}$$

$$v_2 = -\frac{1}{6n}\frac{\partial^2 p_2}{\partial x^2}(y^3 - 3y + 2) - \frac{1}{2}\frac{\partial M_2}{\partial x}(y^2 - 2y + 1). \tag{4.48}$$

putting (4.45) and (4.47) into (4.7) we can obtain,

$$\frac{\partial h}{\partial t} + \frac{\partial \mathscr{R}}{\partial x} = 0, \quad \text{at} \quad y = h(x,t), \tag{4.49}$$

here,

$$\mathscr{R} = \frac{1}{6}\frac{\partial p_1}{\partial x}h^3 + \frac{1}{2}M_1 h^2, \quad \text{at} \quad y = h(x,t), \tag{4.50}$$

where M_i can be determined by using (4.6) and (4.25) then using first term of (4.27). Their expressions are simplified to

$$M_2 = \frac{1}{n}\left[M_1 - h\frac{\partial f}{\partial x}\right], \quad M_1 = \frac{-\left[1 + (n-1)h^2\right]\frac{\partial p_1}{\partial x} - (h-1)^2\frac{\partial f}{\partial x}}{2\left[1 + (n-1)h\right]}. \tag{4.51}$$

Satisfying, (4.6) is equivalent to solving the flow rate $Q(t)$, defined by (4.37), and this leads to determining the leading order pressure gradient, finding

$$\frac{\partial p_1}{\partial x} = \mathscr{D}^{-1}\left[(h-1)^2[(n-1)h^2 + 2(1-2n)h - 1]\frac{\partial f}{\partial x} - 12n[(n-1)h + 1]Q\right] \tag{4.52}$$

where,

$$\mathscr{D} = n^2h^4 + 2nh(1-h)[2 - h(1-h)] + (1-h)^4 \tag{4.53}$$

putting (4.51) and (4.52) in (4.50), we obtain

$$\mathscr{R} = \mathscr{D}^{-1}\left[nh^2H_1 + \frac{1}{3}h^3H_2\frac{\partial f}{\partial x}\right] \tag{4.54}$$

where,

$$H_1 = [(n-1)h^2 - 2h + 3]Q \quad \text{and} \quad H_2 = [(1-h) + nh](1-h)^3 \tag{4.55}$$

putting (4.54) into (4.49) we obtain the thin film equation

$$\frac{\partial h_{NS}}{\partial t} + \frac{\partial}{\partial x}\left(\mathscr{D}^{-1}\left[nh^2 H_1 + \frac{1}{3}h^3 H_2 \frac{\partial f}{\partial x}\right]\right) = 0 \tag{4.56}$$

The equation (4.56) is similar to the model long-wave evolution equation in [75].

4.3 Asymptotic approximation in the limit $n \to 0$ and $\alpha \to 0$

Taking the limit of (4.39) as $n \to 0$, we obtain

$$\mathscr{R} = \lim_{n\to 0} S(\alpha, n), \quad \text{at} \quad y = h(x,t) \tag{4.57}$$

The RHS of (4.57) can be expanded in a series form to give

$$\lim_{n\to 0} S(\alpha, n) = -\frac{1}{3}h^3\frac{\partial f}{\partial x} + \frac{2\alpha^2}{15}h^5\frac{\partial f}{\partial x} + \alpha^{-4}\left(\frac{36007\alpha^8}{5040} + \frac{-1021\alpha^8}{144}\right)h^7\frac{\partial f}{\partial x} + ... + O(h^8) \tag{4.58}$$

Substituting (4.58) into (4.57), we have

$$\mathscr{R} = -\frac{1}{3}h^3\frac{\partial f}{\partial x} + \frac{2\alpha^2}{15}h^5\frac{\partial f}{\partial x} - \frac{17\alpha^4}{315}h^7\frac{\partial f}{\partial x} + ..., \quad \text{at} \quad y = h(x,t) \tag{4.59}$$

In the absence of surface tension, we can have

$$\frac{\partial f}{\partial x} = \tilde{B}\frac{\partial h}{\partial x} \tag{4.60}$$

considering (3.27) and (4.60) implies that,

$$\frac{\partial p}{\partial x} = \frac{\partial f}{\partial x} \tag{4.61}$$

Thus the equation (4.57) becomes,

$$\mathscr{R} = -\left[\frac{1}{3}h^3 - \frac{2}{15}h^5\alpha^2 + \frac{17}{315}h^7\alpha^4 - ...\right]\frac{\partial p}{\partial x} \tag{4.62}$$

Now, (4.62) is equivalent to (3.40), also (3.40) is the expansion of (3.32).

Therefore the equation (4.57) becomes

$$\mathscr{R} = -\frac{1}{\alpha^2}\frac{\partial p}{\partial x}\left[\frac{1}{\alpha}\tanh(\alpha h) - h\right], \quad at \quad y = h(x,t). \tag{4.63}$$

Substituting (4.63) into (4.33), we obtain a thin film equation

$$\frac{\partial h_{DB}}{\partial t} = \tilde{B}\frac{\partial}{\partial x}\left[\frac{1}{\alpha^2}\left(\frac{1}{\alpha}\tanh(\alpha h) - h\right)\frac{\partial h}{\partial x}\right]. \tag{4.64}$$

Similarly, if we take the limit of (4.39) as $\alpha \to 0$, we have

$$\mathscr{R} = \lim_{\alpha\to 0} S(\alpha, n), \quad \text{at} \quad y = h(x,t) \tag{4.65}$$

This implies that,

$$\lim_{\alpha\to 0} S(\alpha, n) = -\frac{6Qn(n-1) + [-2(n-1)h^3 + 3(n-2)h - n + 4]\dfrac{\partial f}{\partial x}}{6[(n-1)h^3 + 3h - 2](n-1)}h^3 \tag{4.66}$$

Now, equation (4.65) is simplified to

$$\mathscr{R} = \hat{\mathscr{D}}^{-1}\left[nh^2\hat{H}_1 + \frac{1}{3}h^3\hat{H}_2\frac{\partial f}{\partial x}\right] \quad \text{at} \quad y = h(x,t) \tag{4.67}$$

where,

$$\hat{\mathscr{D}} = [(n-1)h^3+3h-2](n-1), \quad \hat{H}_1 = -Q(n-1)h \quad \text{and} \quad \hat{H}_2 = (n-1)h^3 - \frac{3}{2}(n-2)h + \frac{n}{2} - 2 \tag{4.68}$$

Here we observed that (4.54) and (4.67) have a similar form. Substituting (4.67) into (4.33), we have the thin film equation

$$\frac{\partial h_{NS}}{\partial t} + \frac{\partial}{\partial x}\left(\hat{\mathscr{D}}^{-1}\left[nh^2\hat{H}_1 + \frac{1}{3}h^3\hat{H}_2\frac{\partial f}{\partial x}\right]\right) = 0 \tag{4.69}$$

Now it remains to show that

$$\lim_{\alpha\to 0}\left[\lim_{n\to 0} S(\alpha,n)\right] = \lim_{n\to 0}\left[\lim_{\alpha\to 0} S(\alpha,n)\right] \tag{4.70}$$

The LHS of the (4.70) is

$$\lim_{\alpha\to 0}\left[\lim_{n\to 0} S(\alpha,n)\right] = \lim_{\alpha\to 0}\left(-\frac{1}{\alpha^2}\frac{\partial p}{\partial x}\left[\frac{1}{\alpha}\tanh(\alpha h) - h\right]\right) \tag{4.71}$$

The equation (4.71) has been shown in Section 3.2 which resulted to

$$\lim_{\alpha\to 0}\left[\lim_{n\to 0} S(\alpha,n)\right] = -\frac{1}{3}h^3\frac{\partial p}{\partial x}, \quad \text{at} \quad y = h(x,t) \tag{4.72}$$

The RHS of the (4.70) is

$$\lim_{n\to 0}\left[\lim_{\alpha\to 0} S(\alpha,n)\right] = \lim_{n\to 0}\left(\hat{\mathscr{D}}^{-1}\left[nh^2\hat{H}_1 + \frac{1}{3}h^3\hat{H}_2\frac{\partial f}{\partial x}\right]\right) \tag{4.73}$$

The equation (4.73) is to simplified to

$$\lim_{n\to 0}\left(\hat{\mathscr{D}}^{-1}\left[nh^2\hat{H}_1+\frac{1}{3}h^3\hat{H}_2\frac{\partial f}{\partial x}\right]\right)=-\frac{h^3(h^3-3h+2)}{3(h^3-3h+2)}\frac{\partial f}{\partial x} \tag{4.74}$$

Hence

$$\lim_{n\to 0}\left[\lim_{\alpha\to 0}S(\alpha,n)\right]=-\frac{1}{3}h^3\frac{\partial p}{\partial x},\quad \text{at}\quad y=h(x,t) \tag{4.75}$$

4.4 Numerical results

The lubrication equations (4.40) and (4.56) are solved numerically using a Chebfun method on a domain of $[0,\ L]$, and a variable time step size is found to be sufficient to produce accurate results with sinusoidal, Gaussian and wave packet initial conditions of the form (3.52), (3.53) and (3.54) respectively, where, $b = 0.14$, $h_0 = 0.1$, $h_A = 0.5$, $L = 10$ and m is a frequency. Dirichlet boundary conditions are imposed on both ends of the computational domain, $x = 0$ and $x = L$. The solutions of (4.40) are given in the Figures 4.2, 4.3, 4.4, 4.5, 4.6, and 4.7 .

In Figure 4.2, we present the plot of the surface h of the thin film flow for the solution of (4.40), applying the initial condition (3.52) across various values of n and constant value of α. It is evident from each panel that the wave solution with the highest amplitude corresponds to the initial condition as time progresses. As n increases, the steady-state approaches and aligns with the amplitude of the initial condition as shown in the sub-figures of 4.2a to 4.2f.

Figures 4.3 and 4.4 illustrate a scenario similar to that of Figure 4.2, regarding the surface h of the thin film flow for the solutions of (4.40). This is based on the initial conditions (3.53) and (3.54) respectively, across various values of n and constant value of α.

In Figure 4.5, we show the plot of the surface h of the thin film flow for the solution of (4.40), using the initial condition (3.52) for different values of α and constant value of n.

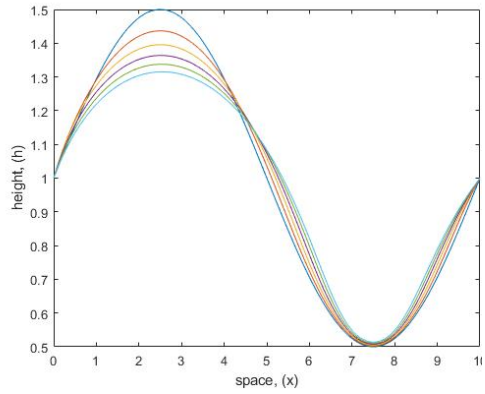

(a) Plot of surface h, with $n = 0$

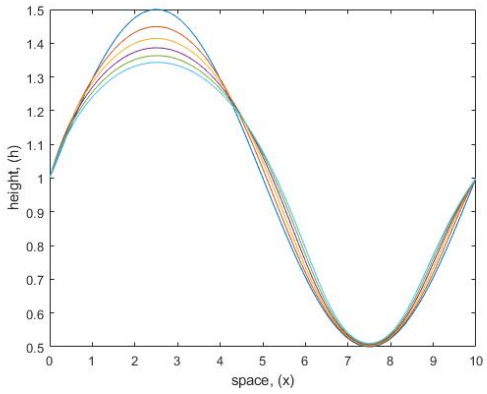

(b) Plot of surface h, with $n = 0.1$

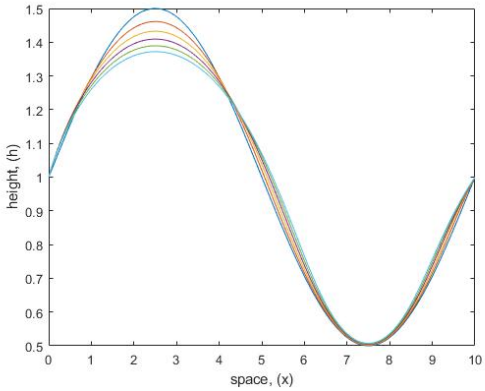

(c) Plot of surface h, with $n = 0.2$

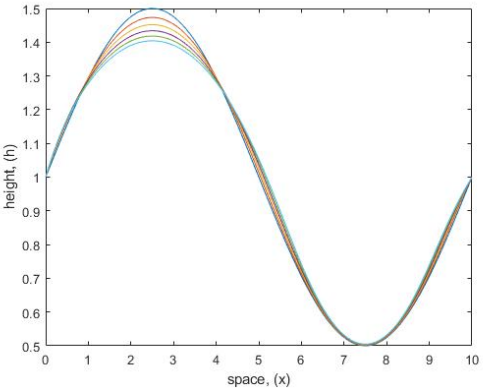

(d) Plot of surface h, with $n = 0.3$

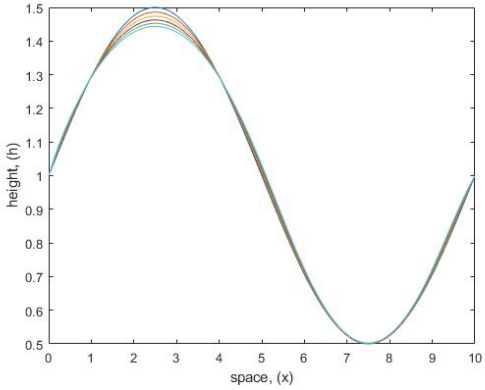

(e) Plot of surface h, with $n = 0.4$

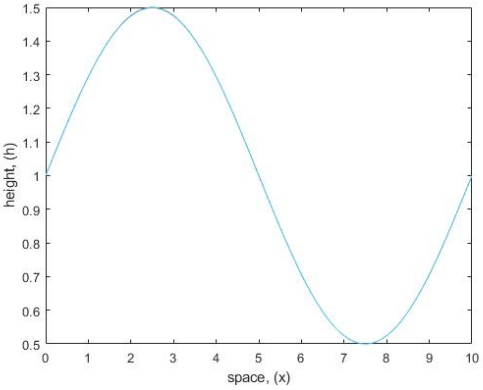

(f) Plot of surface h, with $n = 0.5$

Figure 4.2: Plot of the surface profile h at different times, obtained from a time-dependent calculation of equations (4.40) *with Dirichlet boundary condition, starting from an initial condition of the equation* (3.52)*, with $h_0 = 0.1$, $h_A = 0.5$, $m = 2$, and $L = 10$. The other parameter is $\alpha = 2$. For each panel, display the solution for each value of n as specified in the sub-caption.*

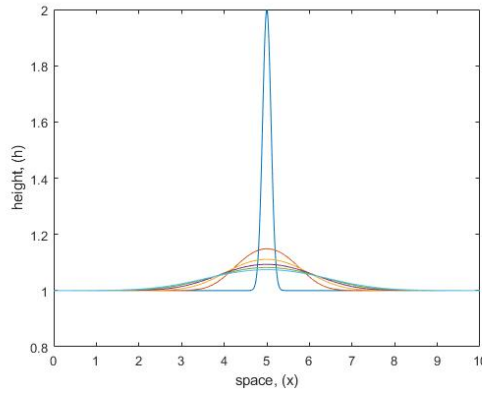

(a) Plot of surface h, with $n = 0$

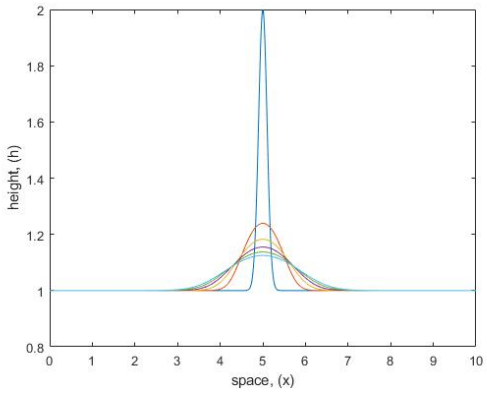

(b) Plot of surface h, with $n = 0.1$

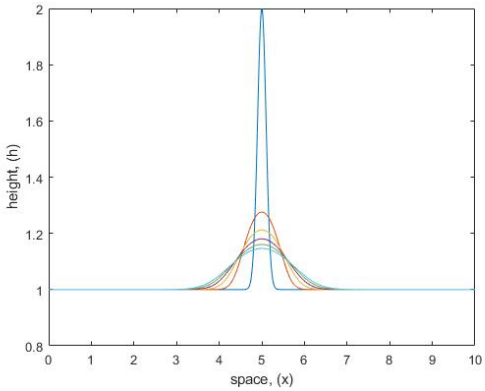

(c) Plot of surface h, with $n = 0.2$

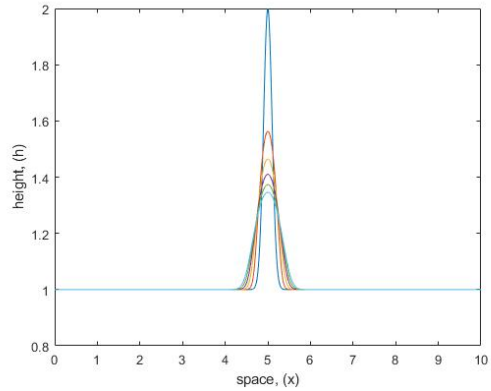

(d) Plot of surface h, with $n = 0.3$

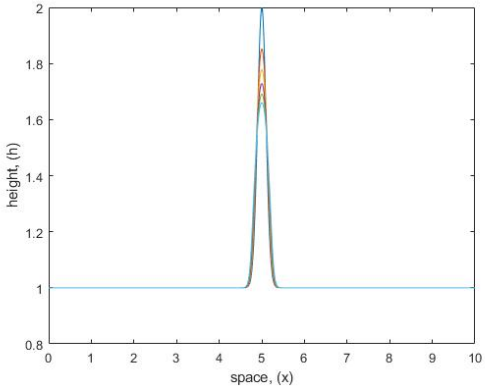

(e) Plot of surface h, with $n = 0.4$

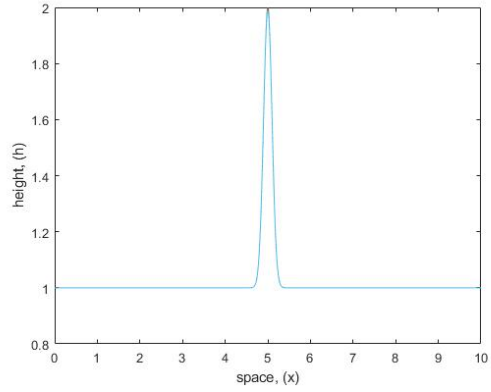

(f) Plot of surface h, with $n = 0.5$

Figure 4.3: Plot of the surface profile h at different times, obtained from a time-dependent calculation of equations (4.40) *with Dirichlet boundary condition, starting from an initial condition of the equation* (3.53)*, with $h_0 = 0.1$, $h_A = 0.5$, $m = 2$, and $L = 10$. The other parameter is $\alpha = 2$. For each panel, display the solution for each value of n as specified in the sub-caption.*

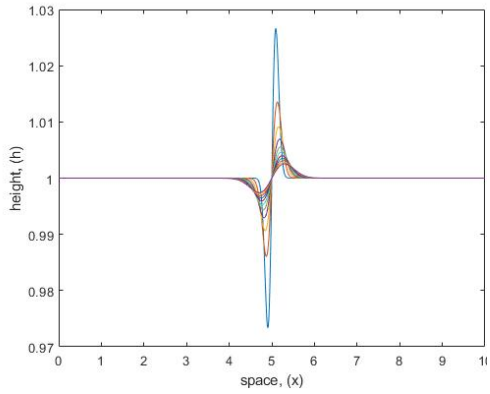

(a) Plot of surface h, with $n = 0$

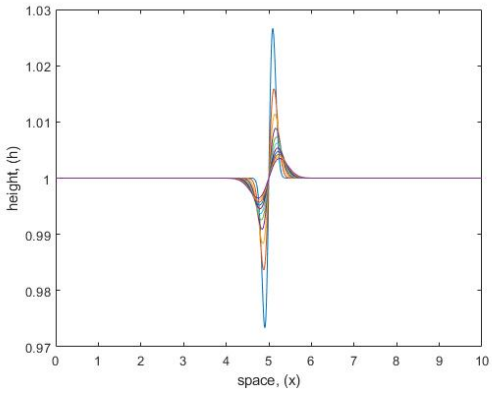

(b) Plot of surface h, with $n = 0.1$

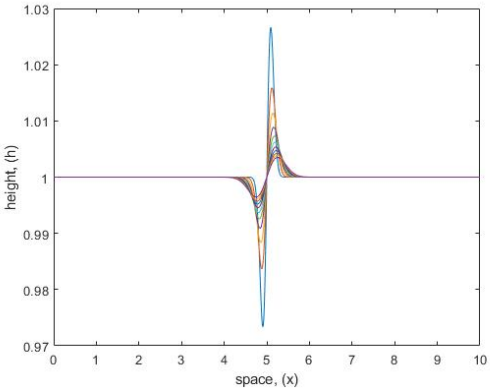

(c) Plot of surface h, with $n = 0.2$

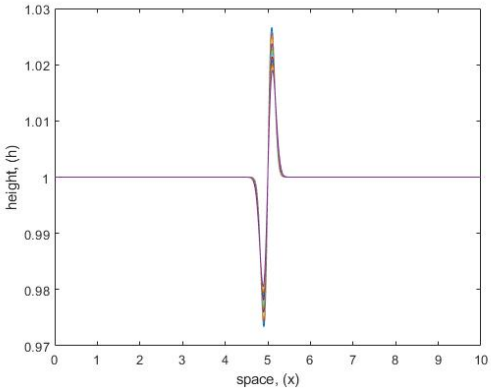

(d) Plot of surface h, with $n = 0.3$

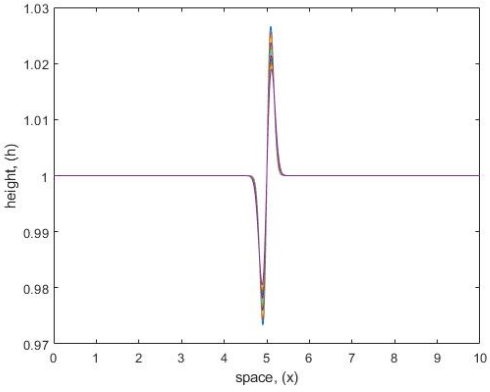

(e) Plot of surface h, with $n = 0.4$

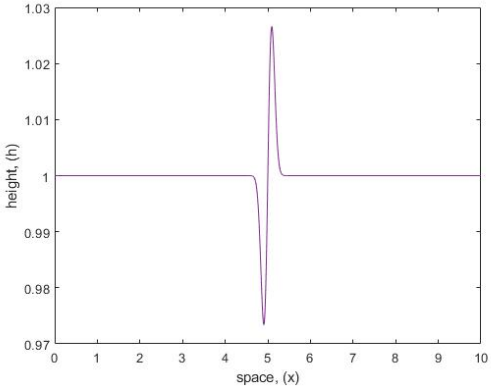

(f) Plot of surface h, with $n = 0.5$

Figure 4.4: Plot of the surface profile h at different times, obtained from a time-dependent calculation of equations (4.40) *with Dirichlet boundary condition, starting from an initial condition of the equation* (3.54)*, with $h_0 = 0.1$, $h_A = 0.5$, $m = 2$, and $L = 10$. The other parameter is $\alpha = 2$. For each panel, display the solution for each value of n as specified in the sub-caption.*

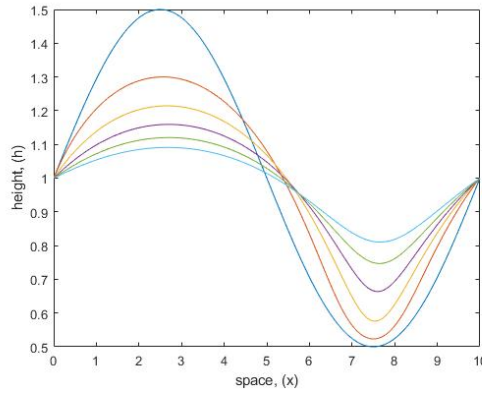

(a) Plot of surface h, with $\alpha = 0$

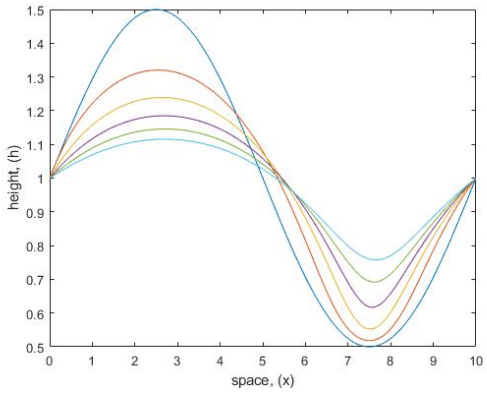

(b) Plot of surface h, with $\alpha = 1$

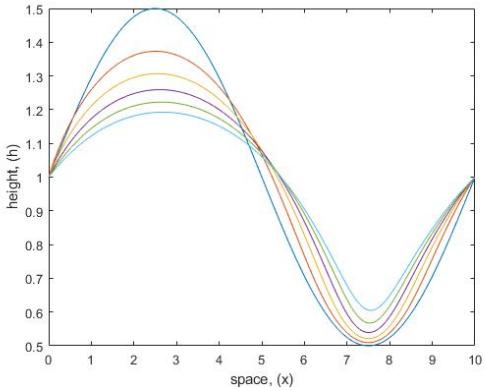

(c) Plot of surface h, with $\alpha = 2$

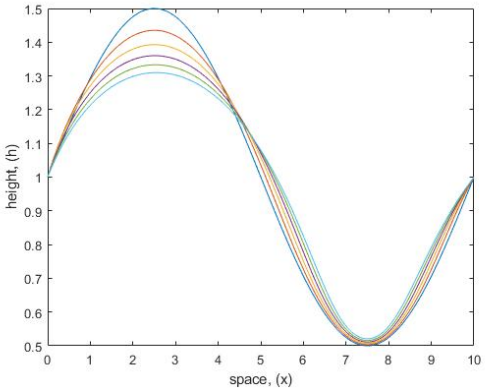

(d) Plot of surface h, with $\alpha = 3$

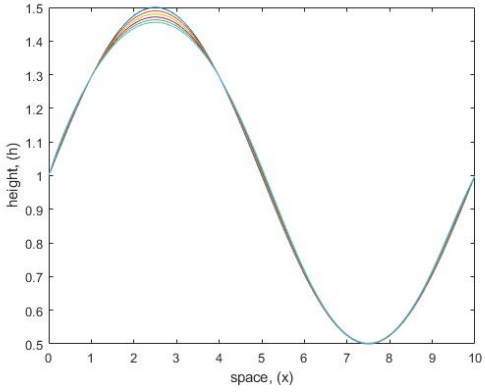

(e) Plot of surface h, with $\alpha = 4$

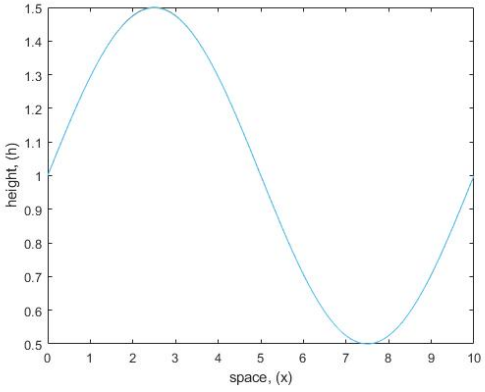

(f) Plot of surface h, with $\alpha = 5$

Figure 4.5: Plot of the surface profile h at different times, obtained from a time-dependent calculation of equations (4.40) *with Dirichlet boundary condition, starting from an initial condition of the equation* (3.52)*, with $h_0 = 0.1$, $h_A = 0.5$, $m = 2$, and $L = 10$. The other parameter is $n = 0.15$. For each panel, present the solution corresponding to each value of α as indicated in the sub-caption.*

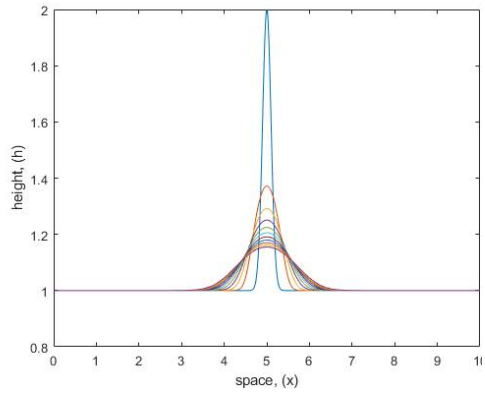

(a) Plot of surface h, with $\alpha = 0$

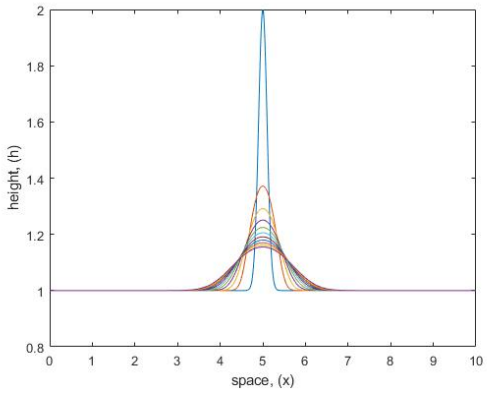

(b) Plot of surface h, with $\alpha = 1$

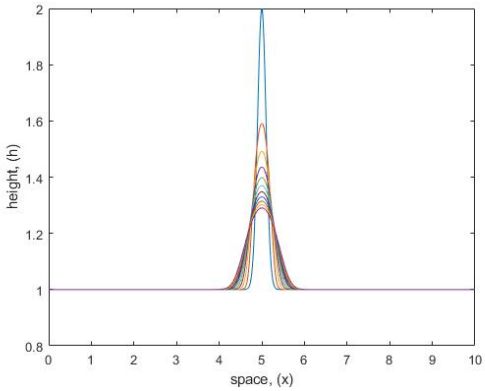

(c) Plot of surface h, with $\alpha = 2$

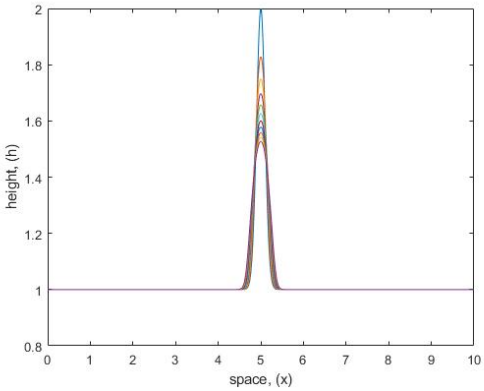

(d) Plot of surface h, with $\alpha = 3$

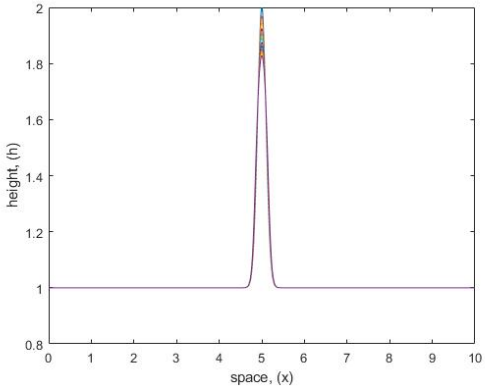

(e) Plot of surface h, with $\alpha = 4$

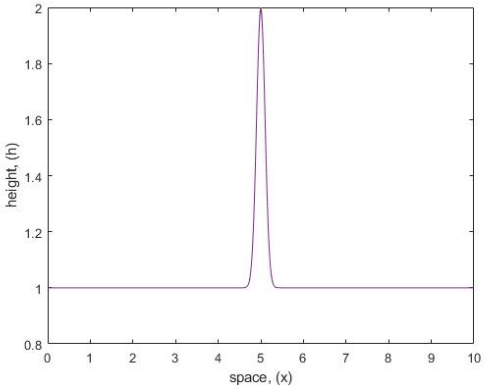

(f) Plot of surface h, with $\alpha = 5$

Figure 4.6: Plot of the surface profile h at different times, obtained from a time-dependent calculation of equations (4.40) *with Dirichlet boundary condition, starting from an initial condition of the equation* (3.53)*, with $h_0 = 0.1$, $h_A = 0.5$, $m = 2$, and $L = 10$. The other parameter is $n = 0.15$. For each panel, present the solution corresponding to each value of α as indicated in the sub-caption.*

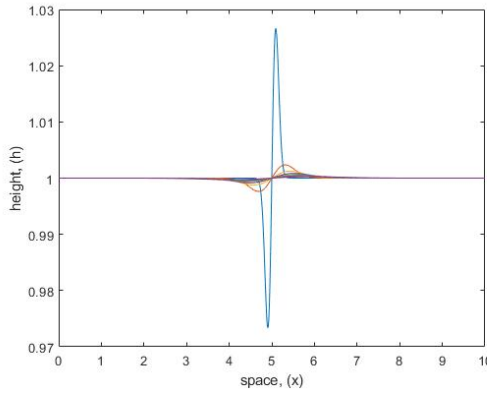

(a) Plot of surface h, with $\alpha = 0$

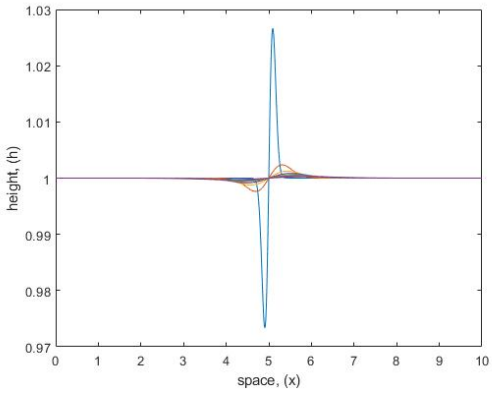

(b) Plot of surface h, with $\alpha = 1$

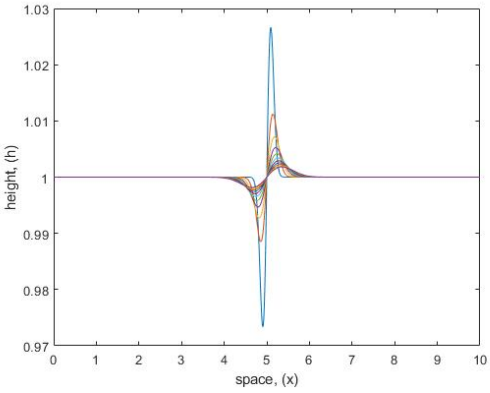

(c) Plot of surface h, with $\alpha = 2$

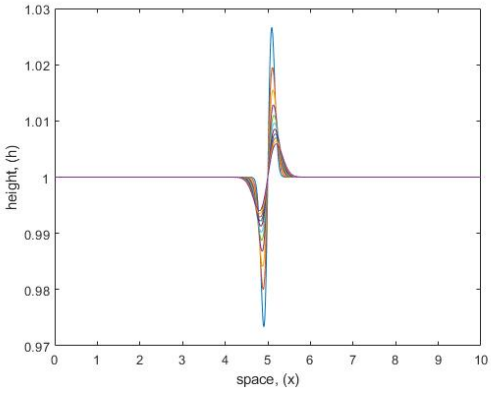

(d) Plot of surface h, with $\alpha = 3$

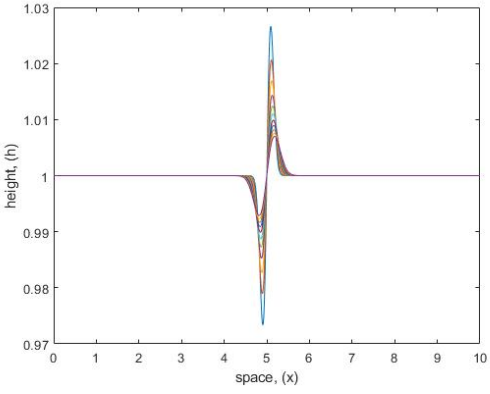

(e) Plot of surface h, with $\alpha = 4$

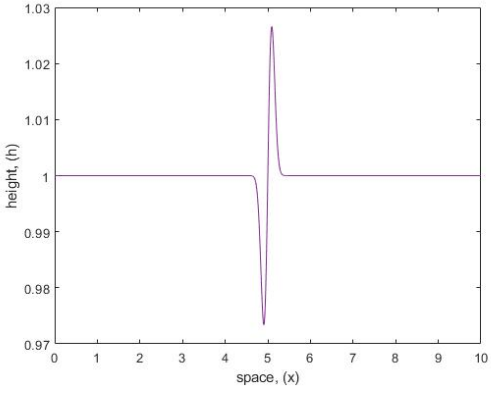

(f) Plot of surface h, with $\alpha = 5$

Figure 4.7: Plot of the surface profile h at different times, obtained from a time-dependent calculation of equations (4.40) *with Dirichlet boundary condition, starting from an initial condition of the equation* (3.54)*, with $h_0 = 0.1$, $h_A = 0.5$, $m = 2$, and $L = 10$. The other parameter is $n = 0.15$. For each panel, present the solution corresponding to each value of α as indicated in the sub-caption.*

Each panel clearly indicates that the wave solution with the greatest amplitude corresponds to the initial condition as time advances. As α increases, the steady-state converges slowly and matches the amplitude of the initial condition, as also illustrated in the sub-figures 4.5a to 4.5f.

Figures 4.6 and 4.7 depict a situation akin to that shown in Figure 4.5, focusing on the surface h of the thin film flow for the solutions of (4.40). This analysis is grounded in the initial conditions (3.53) and (3.54) respectively, across different values of α and constant value of n.

Generally, Figure 4.2 shows that as the value of n increases, the solutions (4.40) evolve more rapidly over time, reaching a quasi-steady state sooner. This causes the profiles at different times to appear closely aligned with the initial condition (3.52), giving the impression that little change has occurred.

Figure 4.5, illustrates that as the value of α goes up, the solution (4.40) of evolution slows down over time. This means that the solution profiles at various moments stay quite close to the initial condition (3.52), making the changes seem minimal.

Likewise, Figures 4.3 and 4.6, which use the initial condition (3.53), along with Figures 4.4 and 4.7 with the initial condition (3.54), exhibit the same pattern.

Chapter 5

Conclusions and Recommendations

5.1 Conclusions

We have developed some models and a series of simulations to describe a flow in a porous medium. In Chapter 3, we presented thin film models of a single fluid's flow in a porous medium bounded by a horizontal ground floor below and a gas phase above. The chapter examines the asymptotic behaviour of the derived thin-film model when α approaches 0 and infinity. In the limit $\alpha \to 0$, the flow in the porous medium behaves similarly to a free surface flow governed by the Navier-Stokes equations. In addition, the limit $\alpha \to \infty$ corresponds to very low permeability k. The flow behaviour aligns with Darcy's Law, describing the classic flow scenario through a porous medium. The numerical simulations confirm that as the value of α increases (meaning the permeability decreases), the flow experiences greater resistance, causing the waves to dampen more quickly and the system to reach a steady state faster. These observations further support that porous media's flow behaviour gradually shifts from a free surface to a Darcy flow regime as the permeability decreases. In Chapter 4, we also presented a thin film model for two immiscible fluids separated by a sharp interface in both porous and non-porous media. The asymptotic analysis in the Chapter shows a connection

between thin film models in porous and non-porous media when the permeability parameter α approaches 0, the thin film equation derived for a porous medium converges to the thin film equation for a non-porous medium. The viscosity ratio n plays an important role in determining the flow dynamics in a two-fluid system. When n is set to 0, the two-fluid thin film model simplifies to a single-fluid model. The numerical simulations show the influence of parameters like permeability and viscosity ratio on the dynamics of the two fluids especially when the two values n and α were increased, their wave formation moving very slowly so they do not move away from the initial condition on the time scale of the numerical simulation.

5.2 Recommendation for future work

After considering the results obtained in the thesis regarding the modelling and simulation of single and two fluids thin film in a porous medium, a few recommendations for further studies are as follows:

- Future research could explore the relationship between the behaviour of a thin film in a porous medium and that of a free surface medium in more detail. These behaviours can converge when a specific parameter α is small, specifically as α approaches zero. Future work could expand upon this by examining a wider range of fluids with different properties and investigating the effects of different porous media structures beyond the current focus on high porosity and permeability.

- Future research could address the limitations of the Brinkman equation. The sources note that the Brinkman equation, which the study uses to model fluid flow through porous media, may not accurately predict flow fields in scenarios involving low porosity. Future work could incorporate more sophisticated models that account for flow complexities in low-porosity environments.

- Future research could examine multi-fluid systems. The sources focus on single-fluid and two-fluid systems with an interface between them. Future work could explore the behaviour of thin films in multi-fluid systems with more complex interfaces and interactions.

- Future research could investigate the suitability of different numerical methods. The sources use Chebfun to simulate the behaviour of thin films in porous media. Future work could explore other numerical methods and compare different approaches to assess accuracy, efficiency, and suitability for specific scenarios.

Appendix A

The exact form of $\Gamma(\alpha, n)$ and $S(\alpha, n)$

From equation (4.38), we have

$$\frac{\partial P_1}{\partial x} = \Gamma(\alpha, n). \tag{A.1}$$

The LHS of A.1 is simplified to be given as

$$\Gamma(\alpha, n) = \frac{\Gamma_N(\alpha, n)}{\Gamma_D(\alpha, n)} \tag{A.2}$$

where,

$$\begin{aligned}\Gamma_N(\alpha,n) = & -e^{\alpha h}e^{-\alpha h}Q\alpha^3n^2 - e^{\alpha h}e^{2\alpha h}Q\alpha^3n - e^{2\alpha h}e^{-\alpha h}\alpha fhn - e^{\alpha h}e^{-\alpha h}\alpha fhn \\ & - e^{3\alpha h}\alpha fhn - e^{2\alpha h}\alpha fhn + e^{2\alpha h}e^{2\alpha h}\alpha fh + e^{2\alpha h}e^{-\alpha h}\alpha fn + e^{(\alpha(h-1))}e^{\alpha h}e^{-\alpha h}fn \\ & + e^{\alpha h}e^{2\alpha h}\alpha fh + e^{\alpha h}e^{-\alpha h}\alpha fn + e^{2\alpha h}e^{-\alpha h}Q\alpha^3n^2 - e^{2\alpha h}e^{2\alpha h}Q\alpha^3n \\ & - e^{4\alpha h}f - e^{2\alpha h}f + 2e^{\alpha h}f - e^{\alpha h}\alpha f + e^{\alpha h}\alpha fh - e^{2\alpha h}\alpha f - Q\alpha^3ne^{\alpha h} \\ & + e^{2\alpha h}e^{-\alpha h}fn + e^{\alpha h}e^{2\alpha h}fn + e^{2\alpha h}\alpha fh - 3e^{\alpha h}e^{-\alpha h}fn - e^{2\alpha h}e^{2\alpha h}\alpha f \\ & - e^{(\alpha(h-1))}e^{\alpha h}e^{2\alpha h}f + e^{(\alpha(h-1))}e^{-\alpha h}fn - e^{\alpha h}e^{2\alpha h}\alpha f + e^{3\alpha h}Q\alpha^3n^2 \\ & + e^{2\alpha h}Q\alpha^3n^2 - e^{2\alpha h}Q\alpha^3n + e^{3\alpha h}\alpha fn + e^{2\alpha h}\alpha fn + e^{(\alpha(h-1))}e^{2\alpha h}fn \\ & - 2e^{2\alpha h}fn + 2e^{\alpha h}e^{2\alpha h}f - e^{(\alpha(h-1))}e^{\alpha h}f + e^{\alpha h}fn - e^{(\alpha(h-1))}fn\end{aligned}$$

$$\begin{aligned}\Gamma_D(\alpha,n) = & e^{\alpha h}\alpha h - 2e^{2\alpha h}n - e^{2\alpha h}e^{2\alpha h}\alpha hn + e^{3\alpha h}\alpha hn^2 - e^{3\alpha h}\alpha hn + e^{\alpha h}e^{-\alpha h}\alpha n \\ & + e^{\alpha h}e^{2\alpha h}\alpha h - 3e^{\alpha h}e^{-\alpha h}n + e^{(\alpha(h-1))}e^{-\alpha h}n + e^{\alpha h}e^{(\alpha(h-1))}n \\ & + e^{2\alpha h}e^{-\alpha h}n + e^{3\alpha h}\alpha n + e^{2\alpha h}e^{(\alpha(h-1))}n - e^{2\alpha h}e^{-\alpha h}n^2 + e^{2\alpha h}\alpha n \\ & - e^{-\alpha h}e^{2\alpha h}n^2 + 2e^{\alpha h}e^{-\alpha h}n^2 - e^{(\alpha(h-1))}e^{2\alpha h}n + e^{2\alpha h}e^{2\alpha h}n \\ & + e^{2\alpha h}e^{2\alpha h}\alpha h + e^{2\alpha h}\alpha hn^2 + e^{2\alpha h}e^{-\alpha h}\alpha n - 2e^{2\alpha h}\alpha hn \\ & + e^{\alpha h}e^{(\alpha(h-1))}e^{-\alpha h}n - \alpha hne^{\alpha h} - e^{2\alpha h}e^{-\alpha h}\alpha hn - e^{\alpha h}e^{-\alpha h}\alpha hn \\ & + e^{2\alpha h}e^{-\alpha h}\alpha hn^2 + e^{\alpha h}e^{-\alpha h}\alpha hn^2 - e^{\alpha h}e^{2\alpha h}\alpha hn - e^{4\alpha h} + 2e^{\alpha h}e^{2\alpha h} \\ & - e^{(\alpha(h-1))}e^{\alpha h} + 2e^{\alpha h} - e^{2\alpha h} + e^{2\alpha h}\alpha h - e^{2\alpha h}\alpha - e^{\alpha h}\alpha \\ & - e^{2\alpha h}e^{2\alpha h}\alpha - e^{\alpha h}e^{2\alpha h}\alpha - e^{(\alpha(h-1))}e^{\alpha h}e^{2\alpha h} + e^{4\alpha h}n \\ & + 2e^{2\alpha h}2n^2 - ne^{\alpha h} + e^{2\alpha h}n - e^{(\alpha(h-1))}n - e^{3\alpha h}n^2 - e^{\alpha h}e^{2\alpha h}n^2\end{aligned}$$

Also, from the equation (4.39) we have,

$$\mathscr{R} = S(\alpha,n) \quad \text{at} \quad y = h(x,t). \tag{A.3}$$

The LHS of (A.3) is also simplified to be define as

$$S(\alpha, n) = \frac{S_N(\alpha, n)}{S_D(\alpha, n)} \tag{A.4}$$

where,

$$\begin{aligned}
S_N(\alpha, n) = {} & 2e^{6\alpha h}\alpha f - 2e^{2\alpha h}\alpha f + e^{2\alpha h} f + f e^{\alpha(6h-1)} + f e^{\alpha(7h-1)} - f e^{\alpha(2h-1)} + f e^{7\alpha h} \\
& - e^{6\alpha h} f - e^{3\alpha h} f - f e^{\alpha(3h-1)} + 2e^{\alpha h} f - 2e^{5\alpha h} f - e^{\alpha h}\alpha f - e^{3\alpha h}\alpha f \\
& + e^{5\alpha h}\alpha f + \alpha f e^{7\alpha h} - h f \alpha^2 e^{7\alpha h} - \alpha f h e^{\alpha(3h-1)} + e^{\alpha h}\alpha^2 f h^2 \\
& - e^{\alpha(2h-1)}\alpha f h + h^2 f \alpha^2 e^{7\alpha h} - e^{5\alpha h}\alpha f h - \alpha f h e^{6\alpha h} \\
& - \alpha f h e^{\alpha(6h-1)} - \alpha f h e^{\alpha(7h-1)} - e^{\alpha h}\alpha^2 f h - 3h f \alpha^2 e^{5\alpha h} \\
& - 2\alpha f h e^{\alpha(5h-1)} + 2e^{4\alpha h}\alpha f h - 4e^{4\alpha h}\alpha^2 f h - 2h f \alpha^2 e^{6\alpha h} \\
& - 2\alpha f h e^{7\alpha h} + 3e^{3\alpha h}\alpha^2 f h^2 - 2e^{\alpha(4h-1)}\alpha f h + 3h^2 f \alpha^2 e^{5\alpha h} \\
& + 2e^{2\alpha h}\alpha^2 f h^2 + 2e^{6\alpha h}\alpha^2 f h^2 + 4e^{4\alpha h}\alpha^2 f h^2 \\
& - 3e^{3\alpha h}\alpha^2 f h + 3e^{\alpha h}\alpha f h - 2e^{2\alpha h}\alpha^2 f h + 3e^{2\alpha h}\alpha f h + 4e^{3\alpha h}\alpha f h
\end{aligned}$$

$$\begin{aligned}
S_D(\alpha, n) = {} & 3e^{3\alpha h}\alpha^4 h + 4e^{4\alpha h}\alpha^4 h + 3e^{5\alpha h}\alpha^4 h + 2e^{2\alpha h}\alpha^4 h + 2e^{6\alpha h}\alpha^4 h \\
& - e^{7\alpha h}\alpha^4 - e^{\alpha h}\alpha^4 + e^{2\alpha h}\alpha^3 + e^{6\alpha h}\alpha^3 - e^{\alpha(3h-1)}\alpha^3 \\
& - e^{\alpha(6h-1)}\alpha^3 - e^{\alpha(7h-1)}\alpha^3 - e^{7\alpha h}\alpha^3 - e^{\alpha(2h-1)}\alpha^3 \\
& - 3e^{3\alpha h}\alpha^4 - 2e^{2\alpha h}\alpha^4 - 4e^{4\alpha h}\alpha^4 - 2e^{6\alpha h}\alpha^4 - 3e^{5\alpha h}\alpha^4 \\
& + 3e^{3\alpha h}\alpha^3 + 2e^{\alpha h}\alpha^3 + 2e^{4\alpha h}\alpha^3 - 2e^{\alpha(5h-1)}\alpha^3 - 2e^{\alpha(4h-1)}\alpha^3 \\
& + e^{7\alpha h}\alpha^4 h + e^{\alpha h}\alpha^4 h
\end{aligned}$$

Bibliography

[1] M. M. Abdulla and S. Pokharel. Analytical models for predicting oil recovery from immiscible co2 injection: a literature review. *Journal of Petroleum Science and Engineering*, 219:111131, 2022.

[2] N. Abdussamie and N. Abdussamie. Flow and transport problems in porous media using cfd. *(AASTMT)*, 2009.

[3] D. J. Acheson. Elementary fluid dynamics, 1991.

[4] M Agelinchaab, M. F Tachie, and D. W Ruth. Velocity measurement of flow through a model three-dimensional porous medium. *Physics of Fluids*, 18(1), 2006.

[5] C. Ancey. Plasticity and geophysical flows: A review. *Journal of non-Newtonian fluid mechanics*, 142(1-3):4–35, 2007.

[6] A. S. Arico, P. Bruce, B. Scrosati, J. Tarascon, and W. Van Schalkwijk. Nanostructured materials for advanced energy conversion and storage devices. *Nature materials*, 4(5):366–377, 2005.

[7] J. K. Arthur. *Flow through and over model porous media with or without inertial effects*. University of Manitoba (Canada), 2012.

[8] R. W. Atherton and G. M. Homsy. On the derivation of evolution equations for interfacial waves. *Chemical Engineering Communications*, 2(2):57–77, 1976.

[9] M. T. Balhoff and M. F Wheeler. A predictive pore-scale model for non-Darcy flow in porous media. *Spe Journal*, 14(04):579–587, 2009.

[10] S. G. Bankoffs. Thin liquid films: Fundamentals and applications, 1990.

[11] D. R. Baral, K. Hutter, and R. Greve. Asymptotic theories of large-scale motion, temperature, and moisture distribution in land-based polythermal ice sheets, a critical review and new developments. *Applied Mechanics Review*, 2001.

[12] V. Barra, S. Afkhami, and L. Kondic. Interfacial dynamics of thin viscoelastic films and drops. *Journal of Non-Newtonian Fluid Mechanics*, 237:26–38, 2016.

[13] G. K. Batchelor. *An introduction to fluid dynamics*. Cambridge University Press, 2000.

[14] J. Bear. *Dynamics of fluids in porous media*. Courier Corporation, 2013.

[15] J. Bear and Y. Bachmat. *Introduction to modeling of transport phenomena in porous media*, volume 4. Springer Science & Business Media, 2012.

[16] G. S. Beavers and D. D. Joseph. Boundary conditions at a naturally permeable wall. *Journal of fluid mechanics*, 30(1):197–207, 1967.

[17] A. Bejan. *Convection heat transfer*. John wiley & sons, 2013.

[18] D. J. Benney. Long waves on liquid films. *Journal of mathematics and physics*, 45(1-4):150–155, 1966.

[19] T. L. Bergman. *Fundamentals of heat and mass transfer*. John Wiley & Sons, 2011.

[20] A. L. Bertozzi. The mathematics of moving contact lines in thin liquid films. *Notices of the AMS*, 45(6):689–697, 1998.

[21] A. L. Bertozzi and M. Pugh. The lubrication approximation for thin viscous films: Regularity and long-time behavior of weak solutions. *Communications on pure and applied mathematics*, 49(2):85–123, 1996.

[22] A. S. Bharadwaj, J. Kuhnert, S. P. Bordas, and P. Suchde. A discrete droplet method for modeling thin film flows. *Applied Mathematical Modelling*, 112:486–504, 2022.

[23] A. S. Bharadwaj, E. Thiel, and P. Suchde. A Lagrangian meshfree model for solidification of liquid thin-films. *Computers & Fluids*, 276:106267, 2024.

[24] A. Birkisson and T. A. Driscoll. Automatic Fréchet differentiation for the numerical solution of boundary-value problems. *ACM Transactions on Mathematical Software (TOMS)*, 38(4):1–29, 2012.

[25] D. Bonn, J. Eggers, J. Indekeu, J. Meunier, and E. Rolley. Wetting and spreading. *Reviews of modern physics*, 81(2):739–805, 2009.

[26] W. Breugem. The influence of wall permeability on laminar and turbulent flows. 2005.

[27] P. Carman. Fluid flow through granular beds. *Trans. Inst. Chem. Eng. London*, 15:150–156, 1937.

[28] S. Céspedes Zuluaga. Computational fluid dynamics as a tool for the design of micromodels for the evaluation of surfactant injection in enhanced oil recovery processes.

[29] C. H. Chan, M. Czubak, and M. M. Disconzi. The formulation of the Navier-Stokes equations on Riemannian manifolds. *Journal of Geometry and Physics*, 121:335–346, 2017.

[30] J. Chan, R. W. Morse, M. A. Meissner, K. M. Dressler, E. T. Hurlburt, G. F. Nellis, and A. Berson. Liquid film flow rate from measurements of disturbance wave characteristics for applications in thin film flow. *Experiments in Fluids*, 65(6):93, 2024.

[31] M. Chandesris and D. Jamet. Boundary conditions at a planar fluid–porous interface for a poiseuille flow. *International Journal of Heat and Mass Transfer*, 49(13-14):2137–2150, 2006.

[32] W. Chen and Y. Wang. A mixed finite element method for thin film epitaxy. *Numerische Mathematik*, 122(4):771–793, 2012.

[33] S. Childress. Viscous flow past a random array of spheres. *The Journal of Chemical Physics*, 56(6):2527–2539, 1972.

[34] S. Chun and C. Eskilsson. Method of moving frames to solve the shallow water equations on arbitrary rotating curved surfaces. *Journal of Computational Physics*, 333:1–23, 2017.

[35] A. L. Condorcet and O. Heaviside. Fourier's law of heat conduction. *SELECTED BOOKS BY*, page 229, 2008.

[36] C. Connelly. *A history of Ohm's Law: investigating the flow of electrical ideas through the instruments of their production.* PhD thesis, 2023.

[37] R. V. Craster and O. K. Matar. On the dynamics of liquid lenses. *Journal of colloid and interface science*, 303(2):503–516, 2006.

[38] R. V. Craster and O. K. Matar. Dynamics and stability of thin liquid films. *Reviews of modern physics*, 81(3):1131, 2009.

[39] K. D. Danov, N. Alleborn, H. Raszillier, and F. Durst. The stability of evaporating thin liquid films in the presence of surfactant. i. lubrication approximation and linear analysis. *Physics of Fluids*, 10(1):131–143, 1998.

[40] A. M. Davis and D. F. James. Penetration of shear flow into an array of rods aligned with the flow. *The Canadian Journal of Chemical Engineering*, 82(6):1169–1174, 2004.

[41] P. De Gennes. Wetting: statics and dynamics. *Reviews of modern physics*, 57(3):827, 1985.

[42] M. De Ghislain. Quantitative hydrogeology; groundwater hydrology for engineers. 1986.

[43] S. Dhanekar and S. Jain. Porous silicon biosensor: Current status. *Biosensors and bioelectronics*, 41:54–64, 2013.

[44] T. H. Dracos. Multiphase flow in porous media. In *Modelling and applications of transport phenomena in porous media*, pages 195–220. Springer, 1991.

[45] L. Durlofsky and J. F. Brady. Analysis of the Brinkman equation as a model for flow in porous media. *Physics of Fluids*, 30(11):3329, 1987.

[46] J. C. Eijkel and A. Van Den Berg. Water in micro-and nanofluidics systems described using the water potential. *Lab on a Chip*, 5(11):1202–1209, 2005.

[47] R. Ellahi. Recent trends in coatings and thin film: Modeling and application, 2020.

[48] E. D. Fernández-Nieto, P. Noble, and J. Vila. Shallow water equations for non-Newtonian fluids. *Journal of Non-Newtonian Fluid Mechanics*, 165(13-14):712–732, 2010.

[49] K. F. Freed and M. Muthukumar. On the Stokes problem for a suspension of spheres at finite concentrations. *The Journal of Chemical Physics*, 68(5):2088–2096, 1978.

[50] T. Fries. Higher-order FEM for incompressible Navier-Stokes flow on manifolds. *International journal for numerical methods in fluids*, 88(2):55–78, 2018.

[51] M. M. Gabriella. Flow in fractured media: A Darcy-Stokes-Brinkman modelling approach. 2018.

[52] D. Gallez. Nonlinear instability of biological membrane surfaces with application to bioadhesion. In *Surface Chemistry and Electrochemistry of Membranes*, pages 975–1012. CRC Press, 1999.

[53] G. M. Geise, H. Lee, D. J. Miller, B. D. Freeman, J. E. McGrath, and D. R. Paul. Water purification by membranes: the role of polymer science. *Journal of Polymer Science Part B: Polymer Physics*, 48(15):1685–1718, 2010.

[54] R. C. Givler and S. A. Altobelli. A determination of the effective viscosity for the Brinkman–Forchheimer flow model. *Journal of Fluid Mechanics*, 258:355–370, 1994.

[55] P. J. Goulet and R. F. Aroca. Distinguishing individual vibrational fingerprints: Single-molecule surface-enhanced resonance raman scattering from one-to-one binary mixtures in langmuir- blodgett monolayers. *analytical chemistry*, 79(7):2728–2734, 2007.

[56] R. W. Griffiths. The dynamics of lava flows. *Annual review of fluid mechanics*, 32(1):477–518, 2000.

[57] B. J. Gross and P. J Atzberger. Hydrodynamic flows on curved surfaces: Spectral numerical methods for radial manifold shapes. *Journal of Computational Physics*, 371:663–689, 2018.

[58] J. B. Grotberg. Pulmonary flow and transport phenomena. *Annual review of fluid mechanics*, 26(1):529–571, 1994.

[59] J. B. Grotberg. Respiratory fluid mechanics and transport processes. *Annual review of biomedical engineering*, 3(1):421–457, 2001.

[60] J. B. Grotberg and O. E. Jensen. Biofluid mechanics in flexible tubes. *Annu. Rev. Fluid Mech.*, 36(1):121–147, 2004.

[61] I. Harmony. 2016v3 single-user help-pdf. *Last revised: February*, 24:64–104, 2020.

[62] E. J. Hinch. An averaged-equation approach to particle interactions in a fluid suspension. *Journal of Fluid Mechanics*, 83(4):695–720, 1977.

[63] I. Howells. Drag due to the motion of a Newtonian fluid through a sparse random array of small fixed rigid objects. *Journal of Fluid Mechanics*, 64(3):449–476, 1974.

[64] M. K. Hubbert. Darcy's law and the field equations of the flow of underground fluids. *Transactions of the AIME*, 207(01):222–239, 1956.

[65] H. E Huppert. Gravity currents: a personal perspective. *Journal of Fluid Mechanics*, 554:299–322, 2006.

[66] Herbert E Huppert and Andrew W Woods. Gravity-driven flows in porous layers. *Journal of Fluid Mechanics*, 292:55–69, 1995.

[67] M. Ishii and T. Hibiki. *Thermo-fluid dynamics of two-phase flow*. Springer Science & Business Media, 2010.

[68] N. Issaadi, A. Aït-Mokhtar, R. Belarbi, and A. Hamami. Effect of variability of porous media properties on drying kinetics: application to cement-based materials. In *Advances in Multi-Physics and Multi-Scale Couplings in Geo-Environmental Mechanics*, pages 243–289. Elsevier, 2018.

[69] D. F. James and A. M. Davis. Flow at the interface of a model fibrous porous medium. *Journal of Fluid Mechanics*, 426:47–72, 2001.

[70] T. Jankuhn, M. A. Olshanskii, and A. Reusken. Incompressible fluid problems on embedded surfaces: modeling and variational formulations. *Interfaces and Free Boundaries*, 20(3):353–377, 2018.

[71] H. Jiang, B. Guo, and M. L. Brusseau. Pore-scale modeling of fluid-fluid interfacial area in variably saturated porous media containing microscale surface roughness. *Water resources research*, 56(1):e2019WR025876, 2020.

[72] R. Jiang and J. Pawliszyn. Thin-film microextraction offers another geometry for solid-phase microextraction. *TrAC Trends in Analytical Chemistry*, 39:245–253, 2012.

[73] E. Kalita and J. Baruah. Environmental remediation. In *Colloidal metal oxide nanoparticles*, pages 525–576. Elsevier, 2020.

[74] A. Kalogirou and M.G. Blyth. The role of soluble surfactants in the linear stability of two-layer flow in a channel. *Journal of Fluid Mechanics*, 873:18–48, 2019.

[75] A. Kalogirou and M.G Blyth. Nonlinear dynamics of unstably stratified two-layer shear flow in a horizontal channel. *Journal of Fluid Mechanics*, 955:A32, 2023.

[76] Anna Kalogirou and Mark G Blyth. Nonlinear dynamics of two-layer channel flow with soluble surfactant below or above the critical micelle concentration. *Journal of Fluid Mechanics*, 900:A7, 2020.

[77] K. Kaneko. Determination of pore size and pore size distribution: 1. adsorbents and catalysts. *Journal of membrane science*, 96(1-2):59–89, 1994.

[78] M. Kasenow. *Applied ground-water hydrology and well hydraulics*. Water Resources Publication, 2001.

[79] M. Kaviany. *Principles of heat transfer in porous media*. Springer Science & Business Media, 2012.

[80] S. Kim and W. B Russel. Modelling of porous media by renormalization of the Stokes equations. *Journal of Fluid Mechanics*, 154:269–286, 1985.

[81] J. Koplik, H. Levine, and A. Zee. Viscosity renormalization in the Brinkman equation. *The Physics of fluids*, 26(10):2864–2870, 1983.

[82] I. V. Koptyug. Mri of mass transport in porous media: Drying and sorption processes. *Progress in Nuclear Magnetic Resonance Spectroscopy*, 65:1–65, 2012.

[83] J. J. Kriegsmann and M. J Miksis. Steady motion of a drop along a liquid interface. *SIAM Journal on Applied Mathematics*, 64(1):18–40, 2003.

[84] Prades M. L. Computational fluid dynamics techniques for fixed-bed biofilm systems modeling: numerical simulations and experimental characterization. 2018.

[85] Dominique Langevin and Dominique Langevin. Thin liquid films. *Emulsions, M. and Foams*, pages 71–127, 2020.

[86] R. E. Larson and J. J. Higdon. Microscopic flow near the surface of two-dimensional porous media. part 1. axial flow. *Journal of Fluid Mechanics*, 166:449–472, 1986.

[87] R. E. Larson and J. J. Higdon. Microscopic flow near the surface of two-dimensional porous media. part 2. transverse flow. *Journal of Fluid Mechanics*, 178:119–136, 1987.

[88] D. H. Lee and R. A. Condrate Sr. Ftir spectral characterization of thin film coatings of oleic acid on glasses: I. coatings on glasses from ethyl alcohol. *Journal of materials science*, 34(1):139–146, 1999.

[89] H. G. Lee, J. Shin, and J. Lee. A second-order operator splitting Fourier spectral method for models of epitaxial thin film growth. *Journal of Scientific Computing*, 71:1303–1318, 2017.

[90] P. Lehmann, I. Neuweiler, J. Vanderborght, and H. Vogel. Dynamics of fluid interfaces and flow and transport across material interfaces in porous media—modeling and observations. *Vadose Zone Journal*, 11(3):vzj2012–0105, 2012.

[91] K. A. Lie. *An introduction to reservoir simulation using MATLAB/GNU Octave: User guide for the MATLAB Reservoir Simulation Toolbox (MRST)*. Cambridge University Press, 2019.

[92] H. Liu, P. R. Patil, and U. Narusawa. On Darcy-Brinkman equation: viscous flow between two parallel plates packed with regular square arrays of cylinders. *Entropy*, 9(3):118–131, 2007.

[93] T. S. Lundgren. Slow flow through stationary random beds and suspensions of spheres. *Journal of fluid mechanics*, 51(2):273–299, 1972.

[94] J. Luo, S. Wen, and P. Huang. Thin film lubrication. part i. study on the transition between ehl and thin film lubrication using a relative optical interference intensity technique. *Wear*, 194(1-2):107–115, 1996.

[95] J. Manafian and C. Teymuri sindi. An optimal homotopy asymptotic method applied to the nonlinear thin film flow problems. *International Journal of Numerical Methods for Heat & Fluid Flow*, 28(12):2816–2841, 2018.

[96] P. Meakin and A. M. Tartakovsky. Modeling and simulation of pore-scale multiphase fluid flow and reactive transport in fractured and porous media. *Reviews of Geophysics*, 47(3), 2009.

[97] D Molenaar. Free-surface stability of a damped thin-film flow. *Journal of Engineering Mathematics*, 65:221–228, 2009.

[98] S. H. Momeni-Masule and A. Malek. Hybrid pseudospectral–finite difference method for solving a 3d heat conduction equation in a sub-micro scale thin film. *Numerical Methods for Partial Differential Equations: An International Journal*, 23(5):1139–1148, 2007.

[99] M. J. Moran, H. N. Shapiro, D. D. Boettner, and M. B. Bailey. *Fundamentals of engineering thermodynamics*. John Wiley & Sons, 2010.

[100] T. G. Myers. Thin films with high surface tension. *SIAM review*, 40(3):441–462, 1998.

[101] G. Neale and W. Nader. Practical significance of Brinkman's extension of Darcy's law: coupled parallel flows within a channel and a bounding porous medium. *The Canadian Journal of Chemical Engineering*, 52(4):475–478, 1974.

[102] R. A. Nelson. *Geologic analysis of naturally fractured reservoirs*, volume 1. Gulf Professional Publishing, 1985.

[103] S. F. Nemadjieu. *Finite volume methods for advection-diffusion on moving interfaces and application on surfactant driven thin film flow*. PhD thesis, Faculty of Mathematics and Natural Sciences, University of Bonn, 2012.

[104] V. Nguyen and W. Park. A free surface flow solver for complex three-dimensional water impact problems based on the vof method. *International Journal for Numerical Methods in Fluids*, 82(1):3–34, 2016.

[105] D. A. Nield and A. Bejan. *Convection in porous media*, volume 3. Springer, 2006.

[106] P. Noble and J. Vila. Thin power-law film flow down an inclined plane: consistent shallow-water models and stability under large-scale perturbations. *Journal of Fluid Mechanics*, 735:29–60, 2013.

[107] P. G. Nutting. Physical analysis of oil sands. *AAPG Bulletin*, 14(10):1337–1349, 1930.

[108] J. A. Ochoa-Tapia and S. Whitaker. Momentum transfer at the boundary between a porous medium and a homogeneous fluid—i. theoretical development. *International Journal of Heat and Mass Transfer*, 38(14):2635–2646, 1995.

[109] W. L. Olbricht. Pore-scale prototypes of multiphase flow in porous media. *Annual review of fluid mechanics*, 28(1):187–213, 1996.

[110] L. Onsager. Reciprocal relations in irreversible processes. i. *Physical review*, 37(4):405, 1931.

[111] G. Ooms, A. Segal, S .Y. Cheung, and R. Oliemans. Propagation of long waves of finite amplitude at the interface of two viscous fluids. *International journal of multiphase flow*, 11(4):481–502, 1985.

[112] A. Oron, S. H. Davis, and S. G. Bankoff. Long-scale evolution of thin liquid films. *Reviews of modern physics*, 69(3):931, 1997.

[113] K. A. Overhoff, K. P. Johnston, J. Tam, J. Engstrom, and R. O. Williams III. Use of thin film freezing to enable drug delivery: a review. *Journal of Drug Delivery Science and Technology*, 19(2):89–98, 2009.

[114] S. B. G O'Brien and L. W. Schwartz. Theory and modeling of thin film flows. *Encyclopedia of surface and colloid science*, 1:5283–5297, 2002.

[115] S. B. G. O'Brien and L. W. Schwartz. Thin film flows: Theory and modeling. *Encyclopedia of Surface and Colloid Science, Taylor, and Francis, Abingdon-on-Thames*, pages 6304–6317, 2006.

[116] J. F. O'Hara, W. Withayachumnankul, and I. Al-Naib. A review on thin-film sensing with terahertz waves. *Journal of Infrared, Millimeter, and Terahertz Waves*, 33:245–291, 2012.

[117] S. K. Pal, Y. Sanyasiraju, and R. Usha. Investigation on the performance of meshfree rbf-based method for the solution of thin film flows over topographies through depth-

averaged momentum integral model. *Journal of Computational Science*, 63:101777, 2022.

[118] Samuel S Pegler, Herbert E Huppert, and Jerome A Neufeld. Fluid injection into a confined porous layer. *Journal of Fluid Mechanics*, 745:592–620, 2014.

[119] R. B. Platte and L. N. Trefethen. Chebfun: a new kind of numerical computing. In *Progress in industrial mathematics at ECMI 2008*, pages 69–87. Springer, 2010.

[120] A. Pototsky, M. Bestehorn, D. Merkt, and U. Thiele. Morphology changes in the evolution of liquid two-layer films. *The Journal of chemical physics*, 122(22):224711, 2005.

[121] A.V. Praseeja and N. Sajikumar. A review on the study of immiscible fluid flow in unsaturated porous media: Modeling and remediation. *Journal of Porous Media*, 22(8), 2019.

[122] B. Ren, T. Yuan, C. Li, K. Xu, and S. Hu. Real-time high-fidelity surface flow simulation. *IEEE Transactions on Visualization and Computer Graphics*, 24(8):2411–2423, 2017.

[123] O. Reynolds. On the theory of lubrication and its application to Mr. Beauchamp tower's experiments, including an experimental determination of the viscosity of olive oil. *Philosophical transactions of the Royal Society of London*, (177):157–234, 1886.

[124] J Rouquerol, D Avnir, D. H. Everett, C. Fairbridge, M. Haynes, N. Pernicone, J. Ramsay, K. Sing, and K. Unger. Guidelines for the characterization of porous solids. In *Studies in surface science and catalysis*, volume 87, pages 1–9. Elsevier, 1994.

[125] J. Rubinstein and S. Torquato. Flow in random porous media: mathematical for-

mulation, variational principles, and rigorous bounds. *Journal of fluid mechanics*, 206:25–46, 1989.

[126] C. Ruyer-Quil and Manneville P. Modeling film flows down inclined planes. *Eur. Phys. J. B*, 6:277–292, 1998.

[127] P. G. Saffman. On the boundary condition at the surface of a porous medium. *Studies in applied mathematics*, 50(2):93–101, 1971.

[128] M. Sahimi. *Flow and transport in porous media and fractured rock: from classical methods to modern approaches*. John Wiley & Sons, 2011.

[129] S. Savović and A. Djordjevich. Finite difference solution of the diffusion equation describing the response and recovery of thin film semiconductor gas sensors. *Sensors and Actuators B: Chemical*, 166:200–204, 2012.

[130] L.W. Schwartz and D. E. Weidner. Modeling of coating flows on curved surfaces. *Journal of engineering mathematics*, 29(1):91–103, 1995.

[131] Y. Shiri and A. Shiri. Numerical investigation of fluid flow instabilities in pore-scale with heterogeneities in permeability and wettability. *Rudarsko-geološko-naftni zbornik*, 36(3), 2021.

[132] W Shyy, M. Francois, H. S. Udaykumar, N. N'dri, and R. Tran-Son-Tay. Moving boundaries in micro-scale biofluid dynamics. *Appl. Mech. Rev.*, 54(5):405–454, 2001.

[133] P. Simon and Y. Gogotsi. Materials for electrochemical capacitors. *Nature materials*, 7(11):845–854, 2008.

[134] J. Šperl and J. Trčková. Permeability and porosity of rocks and their relationship based on laboratory testing.

[135] T. M. Squires and S. R. Quake. Microfluidics: Fluid physics at the nanoliter scale. *Reviews of modern physics*, 77(3):977–1026, 2005.

[136] H. A. Stone, A. D. Stroock, and A. Ajdari. Engineering flows in small devices: microfluidics toward a lab-on-a-chip. *Annu. Rev. Fluid Mech.*, 36(1):381–411, 2004.

[137] X. Sun, M. Sun, K. Takabatake, C. C. Pain, and M. Sakai. Numerical simulation of free surface fluid flows through porous media by using the explicit mps method. *Transport in Porous Media*, 127:7–33, 2019.

[138] C. K. Tam. The drag on a cloud of spherical particles in low Reynolds number flow. *Journal of Fluid Mechanics*, 38(3):537–546, 1969.

[139] R. Tryggvason, G. Scardovelli and S. Zaleski. *Direct numerical simulations of gas-liquid multiphase flows.* Cambridge University Press, 2011.

[140] S. Ulusoy. *The mathematical theory of thin film evolution.* PhD thesis, 2007.

[141] M. Wang, B. Gao, and D. Tang. Review of key factors controlling engineered nanoparticle transport in porous media. *Journal of hazardous materials*, 318:233–246, 2016.

[142] J. R. Werber, C. O. Osuji, and M. Elimelech. Materials for next-generation desalination and water purification membranes. *Nature Reviews Materials*, 1(5):1–15, 2016.

[143] J. F Whidborne. Solving optimal control problems using chebfun. In *2016 UKACC 11th International Conference on Control (CONTROL)*, pages 1–6. IEEE, 2016.

[144] S. Whitaker. Flow in porous media i: A theoretical derivation of Darcy's law. *Transport in porous media*, 1:3–25, 1986.

[145] S. Whitaker. The Forchheimer equation: a theoretical development. *Transport in Porous media*, 25(1):27–61, 1996.

[146] S. Whitaker. *The method of volume averaging*, volume 13. Springer Science & Business Media, 2013.

[147] R. D. Wyckoff, H. G. Botset, M. Muskat, and D. W. Reed. The measurement of the permeability of porous media for homogeneous fluids. *Review of Scientific Instruments*, 4(7):394–405, 1933.

[148] B. Zdravkov. Pore classification in the characterization of porous materials: A perspective. *Open Chemistry*, 5(2):385–395, 2007.

[149] D. Zhao, J. Feng, Q. Huo, N. Melosh, G. H. Fredrickson, B. F. Chmelka, and G. D. Stucky. Triblock copolymer syntheses of mesoporous silica with periodic 50 to 300-angstrom pores. *science*, 279(5350):548–552, 1998.

[150] Y. Zhao, H. H. Tan, and B. Zhang. A high-resolution characteristics-based implicit dual time-stepping vof method for free surface flow simulation on unstructured grids. *Journal of Computational Physics*, 183(1):233–273, 2002.

[151] L. Zhou, K. Nyberg, and A. C. Rowat. Understanding diffusion theory and Fick's law through food and cooking. *Advances in physiology education*, 39(3):192–197, 2015.